In Vivo Assessment of Optic Nerve Degeneration in Glaucoma Rat Model using Diffusion Tensor Imaging

E. S. Hui[1,2], S. Q. Fu[3], K. C. Chan[1,2], K. F. So[3], and E. X. Wu[1,2]

[1]Laboratory of Biomedical Imaging and Signal Processing, The University of Hong Kong, Pokfulam, Hong Kong, [2]Department of Electrical and Electronic Engineering, The University of Hong Kong, Pokfulam, Hong Kong, [3]Department of Anatomy, The University of Hong Kong, Pokfulam, Hong Kong

Introduction

Glaucoma is a neurodegenerative disease characterized by visual field loss, cupping of the optic nerve head, and irreversible loss of retinal ganglion cells, and thus their axons [1]. Increase in intraocular pressure (IOP) is believed to be the major risk factor for glaucoma though the disease mechanism is not fully understood yet [1]. A recent study implicated the neural degeneration in intracranial optic nerve, lateral geniculate nucleus and visual cortex in this disease [2]. Clinical diagnosis of glaucoma relies on IOP measurement using tonometer, visual field test and ophthalmoscopy. In this study, we hypothesized that diffusion tensor imaging (DTI) can detect and characterize optic nerve (ON) degeneration during glaucoma disease progression in established animal models. In particular, changes of directional diffusivities may be associated with the gradual loss of axonal density at the ON of the glaucomatous eye. This approach could be valuable for potential MRI assessment of ON integrity in glaucoma patients, and understanding the pathophysiological cascades involved in this disease.

Materials and Methods

Glaucoma Induction: Experimental glaucoma was performed in seven adult female Sprague-Dawley rats (280-300g, N=7) with the detailed procedures described in Ref 3. Briefly, the right eye of each animal was induced with glaucoma by elevating the IOP whereas the left eye served as the control. The episcleral and limbal veins of the right eye were photocoagulated using an Argon laser (Ultima 2000SE Argon Laser, Coherent, USA). A second laser treatment in the same setting was applied 7 days later. This procedure consistently elevated the IOP in the right eye about 1.5 times above normal, which was confirmed by using a Tonopen XL Tonometer (Mentor Massachusetts, The Netherlands).

Diffusion Tensor Imaging: *In vivo* DTI was performed at 8, 10, 12, 14 and 21 days after the first laser treatment. All experiments were performed using a 7-T Bruker scanner (70/16 Bruker PharmaScan, Germany). Diffusion weighted (DW) images were acquired with a respiration-gated spin echo 8-shot EPI readout sequence. An encoding scheme of 30 gradient directions which are homogenously distributed on the unit sphere was used to acquire DW images [4]. The imaging parameters were: TR/TE = 3000/36.5ms, Δ=15ms, δ=5ms, slice thickness = 1mm, FOV = 35mm, data matrix = 256 x 256 (zero filled to 512 x 512), image resolution = 136 x 136 μm^2 and two b-values were used (0 and 1000 s/mm^2). The sequence was repeated four times for signal averaging, resulting in an acquisition time of approximately 90 minutes depending on the respiratory rate. The diffusion tensors were extracted and diagonalized using an in-house Matlab program interfaced to a software for CNLS estimation for DTI (by Dr. CG Koay, STBB/LIMB/NICHD, NIH). Axial diffusivity ($\lambda_{//}$), radial diffusivity ($\lambda_{\perp}$) and fractional anisotropy (FA) were measured in the left and right ON with the identical ROI in all time points. ROI was drawn based on $\lambda_{//}$, $\lambda_{\perp}$ and FA map to avoid covering any CSF. All measurements on the left and right ON were compared using paired t-test, and $p < 0.05$ was considered as significant.

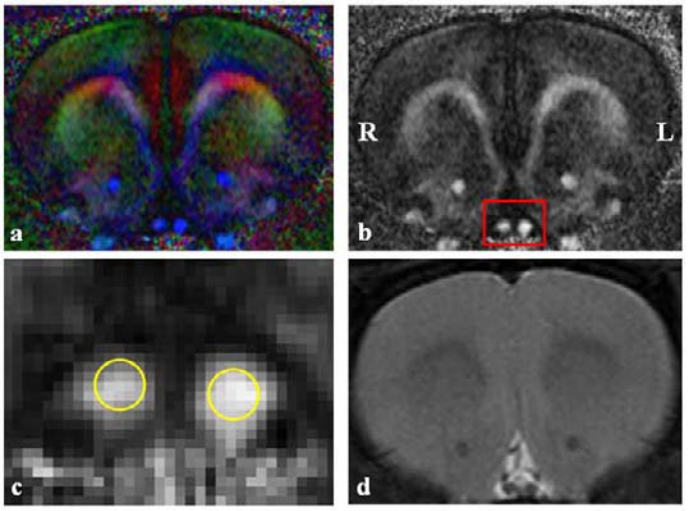

Figure 1. **(a)** Typical color and **(b)** FA map of a glaucoma-induced rat at 21 days after the first laser treatment. **(c)** shows an enlarged view of the optic nerves (ONs) in (b) indicating the obvious difference between the right glaucomatous and left normal ON. ROI was also drawn in (c) to demonstrate the placement for the left and right ON. **(d)** T2-weighted image. R: right, L: left

Results and Discussions

The sequence was tested using a water phantom to demonstrate the general accuracy. At 20^{o}C, the measured apparent diffusion coefficient of water was within 5% error of the value in literature [5] and the water diffusion was isotropic as expected. Fig. 1 shows the typical color, FA map and T2-weighted image of a glaucomatous rat at 21 days after the first laser treatment illustrating the appreciable difference between the right injured and left control ON. As shown in Fig. 2, statistically significant differences were observed between the $\lambda_{\perp}$ and FA of the right and left ON at all time points. However, there was no significant difference for $\lambda_{//}$. $\lambda_{\perp}$ and FA showed increasing and decreasing trend respectively from between day 8 and day 21 after first laser treatment. Given that loss of axons in the ON was observed in previous studies [6], the insignificant $\lambda_{//}$ deviation in the glaucomatous ON suggested that the remaining axons were still largely intact. Furthermore, given that the axonal loss was approximately 19% at 21 days after first laser [6], the corresponding $\lambda_{\perp}$ increase observed here (28%) was likely caused by the axonal density decrease instead of demyelination. Histological analyses are currently under way to validate these *in vivo* DTI observations in the animals studied.

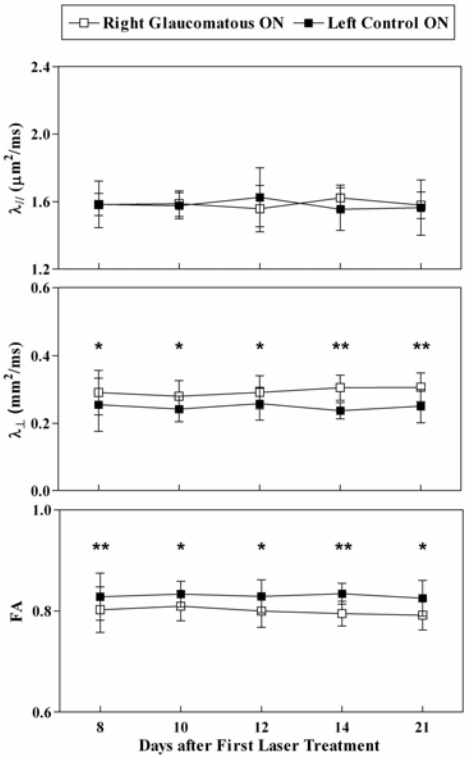

Figure 2. Changes in different DTI parameters, FA, $\lambda_{//}$ and $\lambda_{\perp}$ with respect to time. There is significant difference between left and right ON in all time points for FA and $\lambda_{\perp}$ (N=7). * $p < 0.05$, ** $p < 0.01$

Conclusions

Despite of the high prevalence of the disease, the current clinical measures of function and structure of the visual pathway might not be good surrogates of the neuronal integrity [1]. The present experimental results for the first time indicated that *in vivo* DTI holds promise for diagnosing and assessing glaucoma progression as well as treatment effect. The information obtained from DTI may serve as valuable and reliable indices for evaluating the neuronal integrity and hence the visual pathway.

References

[1] Artes PH et al., Prog. Retin. Eye Res. 2005; 24: 333-54.
[2] Gupta N et al., Br. J. Ophthalmol. 2006; 90: 674-8.
[3] Ji JZ et al., Eur. J. Neurosci. 2004; 19: 265-72.
[4] Jones D et al., Magn. Reson. Med. 1999; 42: 515-525.
[5] Le Bihan D et al., Radiology 1998; 168: 497-505.
[6] Levkovitch-Verbin H, Eye 2004; 18: 1066-1074.

Experimental Eye Research 88 (2009) 65–70

Contents lists available at ScienceDirect

Experimental Eye Research

journal homepage: www.elsevier.com/locate/yexer

Proton magnetic resonance spectroscopy revealed choline reduction in the visual cortex in an experimental model of chronic glaucoma

Kevin C. Chan [a,b], Kwok-fai So [c,d], Ed X. Wu [a,b,c,*]

[a] Laboratory of Biomedical Imaging and Signal Processing, The University of Hong Kong, Pokfulam, Hong Kong
[b] Department of Electrical and Electronic Engineering, The University of Hong Kong, Pokfulam, Hong Kong
[c] Department of Anatomy, The University of Hong Kong, Pokfulam, Hong Kong
[d] The State Key Laboratory of Brain and Cognitive Sciences, The University of Hong Kong, Pokfulam, Hong Kong

ARTICLE INFO

Article history:
Received 5 August 2008
Accepted in revised form 2 October 2008
Available online 1 November 2008

Keywords:
chronic glaucoma
intraocular pressure
visual cortex
proton magnetic resonance spectroscopy
choline
MRI
rat

ABSTRACT

Glaucoma is a neurodegenerative disease of the visual system. While elevated intraocular pressure is considered to be a major risk factor, the primary cause and pathogenesis of this disease are still unclear. This study aims to employ *in vivo* proton magnetic resonance spectroscopy (^{1}H MRS) to evaluate the metabolic changes in the visual cortex in a rat model of chronic glaucoma. Five Sprague–Dawley female rats were prepared to induce ocular hypertension unilaterally in the right eye by photocoagulating the episcleral and limbal veins using an argon laser. Single voxel ^{1}H MRS was performed on each side of the visual cortex 6 weeks after laser treatment. Relative to the creatine level, the choline level was found to be significantly lower in the left glaucomatous visual cortex than the right control visual cortex in all animals. In addition, a marginally significant increase in glutamate level was observed in the glaucomatous visual cortex. No apparent difference was observed between contralateral sides of the visual cortex in T1-weighted or T2-weighted imaging. The results of this study showed that glaucoma is accompanied with alterations in the metabolism of choline-containing compounds in the visual cortex contralateral to the glaucomatous rat eye. These potentially associated the pathophysiological mechanisms of glaucoma with the dysfunction of the cholinergic system in the visual pathway. ^{1}H MRS is a potential tool for studying the metabolic changes in glaucoma *in vivo* in normally appearing brain structures, and may possess direct clinical applications for humans. Measurement of the Cho:Cr reduction in the visual cortex may be a noninvasive biomarker for this disease.

1. Introduction

Glaucoma is a neurodegenerative disease of the visual system characterized by retinal ganglion cell (RGC) death, optic nerve head damage, and progressive visual field loss (Thanos and Naskar, 2004). It is the second major cause of blindness in the world (Quigley and Broman, 2006). While elevated intraocular pressure (IOP) is considered a major risk factor, the primary cause to the atrophic processes is still unclear (Kaufman, 1999). Recently, increasing evidence has been found suggesting the dissemination of glaucomatous damage in the posterior visual pathway in relation to transsynaptic degeneration (Crawford et al., 2000; Duncan et al., 2007; Gupta et al., 2006; Gupta and Yucel, 2003, 2007; Lam et al., 2003; Parisi, 2001; Parisi et al., 2001; Yucel et al., 2003). It has also been demonstrated that exogenous cytidine 5′-diphosphocholine (CDP-choline, or citicoline), which is an intermediate in the generation of phosphatidylcholine (PtdCho) and acetylcholine (ACh) from choline (Cho), may improve visual cortical responses in glaucoma (Parisi, 2005; Parisi et al., 1999; Rejdak et al., 2003). Proton magnetic resonance spectroscopy (^{1}H MRS) has been increasingly utilized to investigate the metabolite distribution in selected volumes of the brain *in vivo* (Babb et al., 2004; Bianchi et al., 2003; Boulanger et al., 2000; Cordoba et al., 2002; Gomez-Anson et al., 2007; Kantarci et al., 2007; Wang et al., 2008; Xu et al., 2005). However, *in vivo* studies of the metabolic changes in human glaucoma are limited (Boucard et al., 2007), possibly due to limited sensitivity and spectral resolution at low magnetic field strengths, limited regional specificity and biological variations between experimental groups. In this study, an experimental glaucoma model was induced by laser photocoagulation of the episcleral and limbal veins in the rat eye, mimicking the pathogenesis of human primary open-angle glaucoma (Li et al., 2006b). As more than 98.5% of the RGC axons in rats decussate to the contralateral visual cortex at the optic chiasm (Fleming et al., 2006), the contralateral visual

* Correspondence to: Ed X. Wu, Laboratory of Biomedical Imaging and Signal Processing, Department of Electrical and Electronic Engineering, The University of Hong Kong, Pokfulam, Hong Kong. Tel.: +852 2819 9713; fax: +852 2819 9711.
E-mail address: ewu@eee.hku.hk (E.X. Wu).

0014-4835/$ – see front matter © 2008 Elsevier Ltd. All rights reserved.
doi:10.1016/j.exer.2008.10.002

cortex receiving input from the treated eye can be compared to the ipsilateral visual cortex receiving input from the intact eye, minimizing biological variations from between-group comparisons. Given that the *in vivo* Cho resonance reflects the abundance of Cho, phosphocholine (PCho), glycerophosphocholine (GPC), ACh, and other Cho compounds (Dowling et al., 2001), this study employs *in vivo* high-field ^{1}H MRS to evaluate the metabolic changes in normally appearing brain structures in a rat model of chronic glaucoma. In particular, we aim to test the hypothesis that alterations in the metabolism of Cho-containing compounds may occur in the visual cortex in chronic glaucoma.

2. Methods

2.1. Animal preparation

Sprague–Dawley female rats (250–280 g, $N = 5$) were reared in a temperature-controlled room subjected to a 12 h light/12 h dark cycle with standard chow and water supply *ad libitum*. They were prepared to induce ocular hypertension unilaterally in the right eye by photocoagulation of the episcleral and limbal veins using an argon laser. A second laser treatment in the same settings was applied 7 days later to block the neovascular flow. This technique has been adopted in our laboratory for the study of retinal and optic nerve degeneration (Chan et al., 2008b, 2007; Hui et al., 2007; Li et al., 2006a,b) as well as ocular transport (Chan et al., 2008a,b, 2007). The IOPs of the glaucomatous and control eyes were measured using a calibrated tonometer (Tonopen-XL, Mentor, Norwell, MA, USA), and were found to be 13.50 ± 0.90 mmHg and 13.56 ± 0.57 mmHg respectively before laser treatments ($p = 0.93$), and 23.07 ± 2.15 mmHg and 13.42 ± 1.07 mmHg respectively after two laser treatments ($p < 0.001$). This IOP elevation by about 1.7 times above the normal level was shown to be maintained up to a maximum of 12-week experimental period (Li et al., 2006a,b). After each procedure, antibiotic ointment was applied topically to the eye surface. Six weeks after laser treatment, ^{1}H MRS was performed at the visual cortex. Throughout the experiments, the left eye and the right visual cortex served as the internal control.

2.2. MRI protocols

All MRI measurements were acquired on a 7 T MRI scanner with a maximum gradient of 360 mT/m (70/16 PharmaScan, Bruker Biospin GmbH, Germany) using a 72 mm birdcage transmit-only RF coil with an actively decoupled receive-only quadrature surface coil. The rat was placed onto a head holder comprising a tooth bar. Under inhaled isoflurane anaesthesia (3% induction and 1.5% maintenance), the animal was kept warm under circulating water at 37 °C. Scout images were first acquired in three planes with a fast spin echo (FSE) sequence to position the subsequent multi-parametric MR images along standard anatomical orientations in a reproducible manner. 2D T1-weighted imaging (T1WI) using FSE sequence was acquired with FOV = 3.2 × 3.2 cm^2, matrix resolution = 256 × 256, slice thickness = 1 mm, number of slices = 10, TR/TE = 400/7.5 ms, echo train length = 4 and NEX = 16; T2-weighted imaging (T2WI) was performed under the same dimensions with TR/TE = 4200/38.7 ms, echo train length = 8 and NEX = 2; for ^{1}H MRS, a 4 × 1 × 4 mm^3 voxel was placed over each side of the visual cortex. The volume of interest was maximized to obtain higher signal-to-noise ratios and to cover the gray matter predominantly in the visual cortex, while avoiding the margins of the white matter structures, which were clearly distinguishable in T2WIs underneath the cortex. After first- and second-order localized voxel shimming with fast automatic shimming technique b mapping along projections (FASTMAP) (Gruetter, 1993), a full-width half-maximum linewidth of water signal of ≤20 Hz would be achieved. The water signal was suppressed by variable power RF pulses with optimized relaxation delays (VAPOR). Outer volume suppression (OVS) combined with point-resolved spectroscopy (PRESS) sequence was used for signal acquisition, with TR/TE = 2000/20 ms, spectral bandwidth = 4 kHz, 2048 data points and 128 averages.

2.3. Data analysis

The morphology in T1WI and T2WI was assessed qualitatively in the visual cortex between contralateral sides. Regions of interest (ROIs) were then drawn manually on each side of the visual cortex covered by the single voxel in ^{1}H MRS using ImageJ v1.40g (Wayne Rasband, NIH, USA) with reference to the rat brain atlas (Paxinos and Watson, 2007). Each value was calibrated to the nearby phantom containing saline solution to avoid the effect of any MRI system sensitivity drift.

The *in vivo* MR spectra were processed using the jMRUI software (version 3.0, http://www.mrui.uab.es/mrui/) (Ratiney et al., 2005). The signal of residual water was filtered with Hackel–Lanczos Singular Value Decomposition (HLSVD) algorithm preprocessing with 25 spectral components for modeling. In addition, a Gaussian apodization of 15 Hz was applied to increase the signal-to-noise ratio of the spectrum. Spectral peaks were assigned in the references of the singlet peak of NAA (CH_3-group). Metabolite areas were estimated using the quantitation based on quantum estimation (QUEST) method combined with subtraction approach for background modeling (Cudalbu et al., 2008). To reduce systematic variations among studied animals and to accurately extract the dominating metabolite changes, a relative quantification method using creatine (Cr) peak as the internal spectral reference was applied. The numerical time-domain modal functions of 10 metabolites [alanine (Ala), aspartate (Asp), Cr, Cho, glutamate (Glu), glycine (Gly), *N*-acetylaspartate (NAA), taurine (Tau), lactate (Lac) and myo-inositol (mI)] were used as prior knowledge in QUEST. These metabolite model signals were quantum mechanically simulated in NMR spectra calculation using operators (NMR-SCOPE) for the *in vivo* experimental protocol. NAA:Cr, Cho:Cr, Glu:Cr, Lac:Cr, and Tau:Cr ratios were statistically evaluated. The reliability of metabolite quantitation was assessed using the Cramer-Rao lower bounds (CRLB) (Cudalbu et al., 2008). An estimate was considered as relevant when the corresponding bound was found below 25% of the estimate. The mean of the relevant estimates and the corresponding error values were computed.

Unless otherwise stated, all data were presented as mean ± standard deviation (SD). Two-tailed paired Student's *t*-tests were performed between contralateral sides of all measurements. Results were considered significant when $p < 0.05$.

3. Results

Fig. 1 shows the typical T1WI and T2WI of the visual cortex. The normalized signal intensities of T1WI and T2WI were measured to be 0.155 ± 0.014 and 0.441 ± 0.016 respectively in the left glaucomatous visual cortex, and 0.158 ± 0.015 and 0.452 ± 0.021 respectively in the right control visual cortex. No statistically significant difference was observed between contralateral sides of the visual cortex in either T1WI or T2WI ($p > 0.05$). Fig. 2 shows the localization of voxel placements to the visual cortex, and the averaged spectra for ^{1}H MRS. The mean values and the corresponding standard deviations of the estimated metabolite ratios were reported in Table 1. In ^{1}H MRS, all 5 animals showed a lower Cho:Cr ratio in the left glaucomatous visual cortex than in the right control visual cortex by 41% ($p < 0.05$). Except for a higher Glu:Cr ratio in the glaucomatous visual cortex with marginal significance ($p = 0.09$), no apparent difference was observed in other

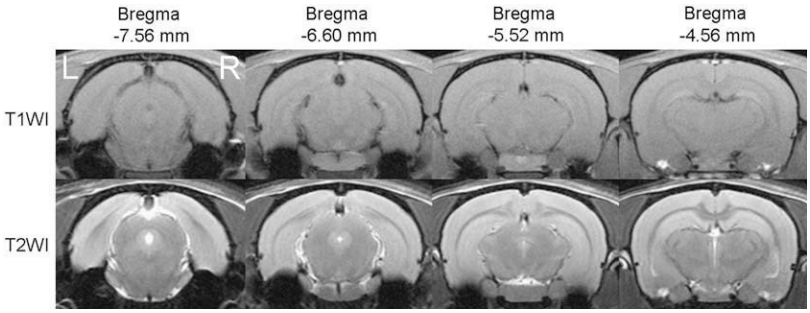

Fig. 1. Typical T1-weighted and T2-weighted images of the visual cortex at Bregma −7.56 mm to −4.56 mm. No apparent difference was observed between contralateral sides of the visual cortex.

metabolites between contralateral sides of the visual cortex ($p > 0.1$). Note that most of metabolites were quantified with CRLB of less than 25%.

4. Discussions

The results of the current study showed that glaucoma is accompanied with alterations in the metabolism of Cho-containing compounds in the rat visual cortex 6 weeks after induction of ocular hypertension. In the current glaucoma model, obstruction of aqueous humor outflow is the primary mechanism of pressure elevation analogous to the pathogenesis of human primary open-angle glaucoma. When a persistent elevation of IOP by 1.7 times was maintained in the rat eye of the same model, a 3% RGC loss per week was documented across the 8-week experimental period (Li et al., 2006a,b). Cho signal intensity reflects cytosolic Cho-containing compounds, 98% of which are PCho and GPC. They provide free Cho for the synthesis of the neurotransmitter ACh by choline acetyltransferase (ChAT), and for the storage in membranous PtdCho in cholinergic neurons (Boulanger et al., 2000; Kantarci et al., 2007; Michel et al., 2006; Schmidt and Rylett, 1993). The ACh level in different rat brain regions has been shown to correlate with the Cho signal intensity in ^{1}H MRS (Wang et al., 2008), while PtdCho is immobilized in cell membranes and is thus largely invisible to ^{1}H MRS (Miller, 1991). Reduction of Cho-containing compounds in the brain has been demonstrated in human and rodent ^{1}H MRS studies on mitochondrial diseases (Bianchi et al., 2003), Huntington disease (Gomez-Anson et al., 2007), hepatic encephalopathy (Cordoba et al., 2002; Taylor-Robinson et al., 1994), stable mild cognitive impairments (Kantarci et al., 2007), and after muscarinic agonist treatment in Alzheimer's disease (Satlin et al., 1997), and is shown to associate with less synthetic activity (Ende et al., 2001), impaired intraneuronal signaling mechanisms (Moore et al., 2000), decreased membrane turnover, and lower cellular density (Dowling et al., 2001). For glaucoma, it is likely the Cho:Cr reduction was a result of reduced cortical activity in addition to transsynaptic degeneration, and was partially associated with the dysfunction of the cholinergic system in the visual pathway.

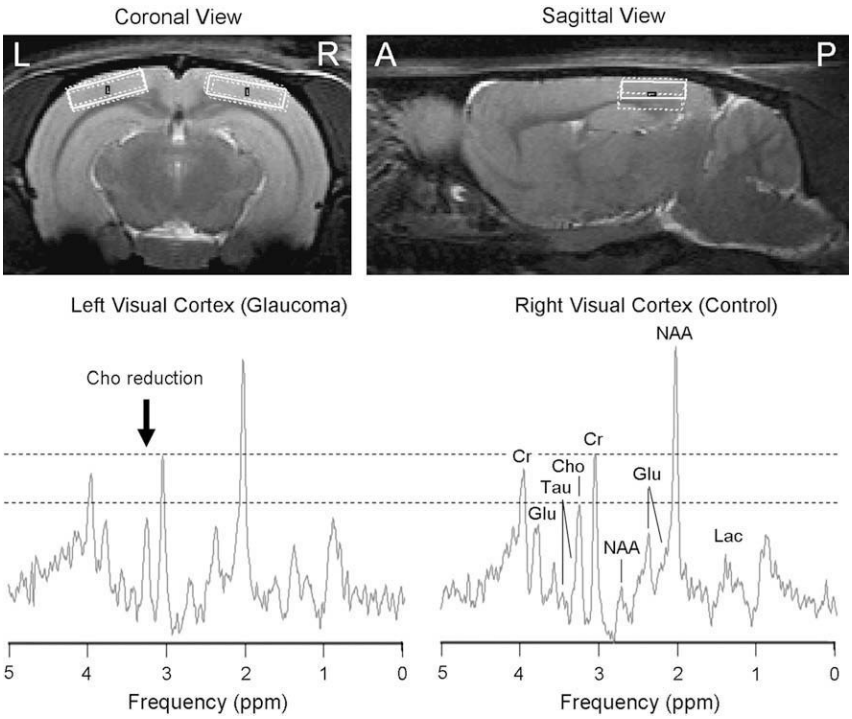

Fig. 2. (Top row) Illustration of the localization of the $4 \times 1 \times 4$ mm^3 voxels (solid-line boxes) in the glaucomatous (L) and control (R) rat visual cortex for ^{1}H MRS. (Bottom row) Averaged spectra for single voxel ^{1}H MRS on each side of the visual cortex. Note the apparently lower Cho signal (arrow) with respect to the Cr signal in the left glaucomatous visual cortex than in the right control visual cortex. (L: left; R: right; A: anterior; P: posterior.)

Table 1
Metabolite ratios and the respective Cramer-Rao lower bounds (CRLB) at each side of the visual cortex 6 weeks after glaucoma induction. (ns: not significant.)

Metabolites to creatine (Cr) ($N = 5$)	Left visual cortex (glaucoma)		Right visual cortex (control)		p Value (two-tailed paired t-test)
	Mean ± SD	Mean % SD (CRLB)	Mean ± SD	Mean % SD (CRLB)	
N-acetyl-aspartate (NAA)	1.36 ± 0.15	5.83 ± 0.38	1.28 ± 0.10	5.28 ± 0.76	ns
Choline (Cho)	0.16 ± 0.05	15.85 ± 4.81	0.27 ± 0.04	8.67 ± 0.92	<0.05
Glutamate (Glu)	1.44 ± 0.33	7.43 ± 1.63	0.96 ± 0.31	8.54 ± 1.89	ns (0.09)
Lactate (Lac)	0.52 ± 0.11	15.92 ± 4.03	0.38 ± 0.15	22.80 ± 8.88	ns
Taurine (Tau)	0.44 ± 0.13	16.84 ± 7.08	0.35 ± 0.24	19.02 ± 9.80	ns

Cholinergic neurons use Cho for the synthesis of the neurotransmitter, ACh, which plays a crucial role in synaptic transmission. In addition, release of ACh is a marker of activation of the primary visual cortex during visual stimulation (Fournier et al., 2004; Laplante et al., 2005). Recent functional MRI studies have shown the effect of visual field loss to the functional organization of human primary visual cortex in primary open-angle glaucoma (Duncan et al., 2007). Glaucomatous visually evoked potential abnormalities (Parisi, 2001, 2005; Parisi et al., 2001) and cytochrome oxidase activity decrease (Crawford et al., 2000; Lam et al., 2003; Yucel et al., 2003) in the primary visual cortex have also been observed and ascribed to impaired neural conduction along postretinal visual pathways, due to the dysfunction of the innermost retinal layers containing the RGCs and their fibers upon RGC loss and elevated IOP induced activity changes (Gupta and Yucel, 2003; Yucel et al., 2003). Using electroretinography, the laser-induced ocular hypertension model in the present study also showed a substantial reduction of retinal functions (Li et al., 2006b). Since the animals were exposed in their cages 12 h/day to light over a 6-week period following laser coagulation, the visual stimulation of the left and right cortex would differ over time. Although it has been reported that acute visual stimulations did not cause significant changes in MR spectra in the human occipital lobe (Boucard et al., 2005), it is possible that the long-term effect of the differences in visual stimulation and cortical activation in the treated and control hemispheres may contribute to the reduction in Cho level upon neurodegeneration of the visual system in the glaucoma rat model. The expression of cholinergic receptors in the visual cortex was found to be regulated by visual input activity and functional state of the visual cortex (Gu, 2003). Analogous to the effect of RGC loss in the treated eye on the contralateral visual cortex in the current model, the spontaneous ACh release from chronically undercut areas of mammal visual cortex was found to be considerably lower than from intact areas of cortex (Collier and Mitchell, 1967; Sato et al., 1987). The amount of ACh in visual cortex also significantly decreased at 2 and 4 weeks after unilateral orbital enucleation in adult rats (Kim et al., 1995). Decreased Cho-containing compounds in ^{1}H MRS in the frontal cortex of preclinical carriers of Huntington disease have been shown to correlate to neuropsychological deficits (Gomez-Anson et al., 2007). It has also been postulated that when the cellular requirement for free Cho for ACh synthesis was reduced, e.g. by applying a muscarinic cholinergic agonist, neuronal membrane breakdown and the concentration of membrane catabolic intermediates, such as GPC could be reduced, resulting in a decrease in the brain Cho resonance in ^{1}H MRS (Satlin et al., 1997). Similarly, in the presence of transsynaptic degeneration and less visual stimulation in glaucoma, it is possible the ACh synthesis and storage in the visual cortex would be reduced, leading to fewer requirements for free Cho, less membrane breakdown, and thus a lower Cho:Cr ratio as observed in the current study.

On the other hand, abnormalities in mitochondrial transport and their defective distribution, whether caused by anatomical constraints (Chan et al., 2008b; Hui et al., 2007) or energy depletion (Osborne et al., 2006) along the glaucomatous visual pathway, may lead to local functional and metabolic crises, including Cho reduction (Bianchi et al., 2003), in correlation to a possible impairment of the normal processes of membrane maintenance due to local energy depletion (Carelli et al., 2004). ChAT is the biosynthesis enzyme of ACh, and its concentration reflects the level of cholinergic activity (Wessler et al., 2003). ChAT is shown to undergo anterograde axonal transport along the rat visual pathway (Yasuhara et al., 2003). Research evidence suggests that glaucoma obstructs anterograde axonal transport in RGC axons at the optic nerve head (McKinnon, 2003). Our previous MRI studies also showed reduced anterograde axonal transport of manganese ions along the glaucomatous visual pathway (Chan et al., 2008b, 2007) in addition to reduced fractional anisotropy and increased radial diffusivity in the prechiasmatic optic nerve by diffusion tensor imaging (Hui et al., 2007) in the same experimental glaucoma model. In the contralateral somatosensory cortex, peripheral deafferentation of the sciatic nerve resulted in significant reductions of ChAT activity and high-affinity Cho uptake (Rothe et al., 1990). ChAT and ACh activities were also reduced in the cortex and striatum in human patients and transgenic mouse models of Huntington disease at young ages (Smith et al., 2006; Vetter et al., 2003), whereby Cho resonance was found to decrease in the frontal cortex in preclinical carriers of Huntington disease patients (Gomez-Anson et al., 2007). Reduced trabecular ChAT has been found in congenital glaucoma rats in association with IOP rise (Gatzioufas et al., 2008). Since ACh is mainly synthesized from ChAT, if there's any damage and blockade to the anterograde axonal transport of ChAT along the glaucomatous visual pathway, it is possible that less Cho-containing compounds would be recruited in the visual cortex.

In addition to the synthesis of ACh, cells use Cho as the precursor of certain phospholipids, e.g. PtdCho, for the major constituents of all biological membranes (Michel et al., 2006). The cells were shown to die by apoptosis when deprived of Cho, possibly due to interruption of cell cycling as a result of the decrease in membrane PtdCho concentration (Yen et al., 1999). In the presence of advanced human glaucoma with 50% visual field loss, neurodegeneration was observed in the visual cortex (Gupta et al., 2006). In the current study, there was no significant difference in NAA:Cr representing neuronal integrity between contralateral sides of the visual cortex. This appeared to relate to the fact that there was only approximately 20% of RGC loss being observed between week 4 and week 8 after glaucoma induction in the current model (Li et al., 2006a,b). While target cell loss represents perhaps the most extreme case of a reduction in trophic supply, decreases due to reduced synaptic connectivity or decreased lateral geniculate nucleus and visual cortex activity might also play an important role, especially during early stage of degeneration (Weber et al., 2008). Our results reflected the initial changes in Cho:Cr that may indicate subtle disturbances of neurological function preceding the development of overt glaucoma in the visual cortex.

Recently, it has been demonstrated that exogenous CDP-choline (citicoline) may improve visual cortical responses in patients with glaucoma, yet the mechanism of its actions in the visual system is not entirely understood (Parisi, 2005; Parisi et al., 1999; Rejdak et al., 2003). Once absorbed, citicoline is widely distributed throughout the body, undergoes a quick transformation to Cho and

cytidine, and crosses the blood–brain barrier into the central nervous system (Grieb and Rejdak, 2002; Secades and Lorenzo, 2006). Cho ingestion increases the *in vivo* ^{1}H MRS resonance of Cho-containing compounds in human brain (Babb et al., 2004). ^{1}H MRS also showed an increase in Cho resonance in the brain of young human subjects after single oral doses of CDP-choline (Babb et al., 1996). In addition to its neuroprotective properties on damaged RGCs in mouse culture retina (Oshitari et al., 2002), citicoline is known to increase in some brain areas the levels and enhance the rate of synthesis of ACh, dopamine, noradrenalin, and serotonin (Secades and Lorenzo, 2006). It is likely that a mechanism for citicoline to provide neuroprotective treatment to glaucoma is to normalize and replace the insufficient Cho contents in the glaucomatous visual cortex observed in the current study.

RGC loss in glaucoma has linked to programmed cell death, termed apoptosis. Among the initiating mechanisms described for RGC and optic nerve degeneration, both oxidative injury and glutamate excitotoxicity seen in neurodegenerative disease have been described in transsynaptic degeneration in primate glaucoma (Gupta and Yucel, 2007). In the etiology of glaucoma, inadequate supply of neurotrophic factors may synergize with excitotoxicity (Grieb and Rejdak, 2002). Similarly, Glu, another major excitatory neurotransmitter in the rat visual cortex (Baughman and Gilbert, 1980), is released by neurons upon stimulation, and is then taken up by surrounding glial cells and converted into glutamine by glutamine synthetase in astrocytes, leading to a decrease in Glu concentration (Xu et al., 2005). The marginally significant increase in Glu:Cr in the glaucomatous visual cortex than the control cortex appeared to associate with the fact that less stimulations occurred in the glaucomatous cortex causing less Glu uptake and conversion by glutamine synthetase. It may also be a result of decreased glutamatergic synaptic activity (Fonnum and Lock, 2004). Note that a significant decrease in Glu uptake and glutamine synthetase activity has been observed in the rat glaucomatous retina (Moreno et al., 2005). Worsening of neuropsychological function has also been shown to correlate with an increase in brain Glu/glutamine in hepatic encephalopathy in company with Cho reduction (Cordoba et al., 2002).

Recent studies have indicated that application of brain-derived trophic factor to both the eye and the visual cortex results in increased levels of RGC survival and function that exceed those seen following treatment of the eye alone (Weber et al., 2008). While previous studies on glaucoma focused on eye mainly, the results of the current study further support the recent issues on the need to investigate into the brain changes in glaucoma so as to look for better treatment effects to this disease. More importantly, this *in vivo* spectroscopic method can be readily translated to study human glaucoma and can have direct clinical applications. In the human brain, the cortical sheet contains both gray and white matters in the range of a few microliters, and is vulnerable to larger partial volume effect than the rat visual cortex in both ^{1}H MRS and proton chemical shift imaging (^{1}H CSI) using ordinary clinical MR scanners. Recent studies demonstrated the ability of ^{1}H CSI to quantify metabolite concentrations in mammalian brains at microliter resolution under high magnetic field strengths (Juchem et al., 2005; Mlynarik et al., 2008). Future experiments would possibly enable the differentiation of the effects on Cho concentrations in gray and white matters upon chronically elevated IOP in humans.

5. Conclusion

The results of this study showed that glaucoma is accompanied with alterations in the metabolism of Cho-containing compounds in the visual cortex. The lower Cho signal is potentially a result of reduced ACh release upon transsynaptic degeneration and visual cortical dysfunction. It may also reflect the compromise of the structural integrity of the neuronal membranes before apparent neuronal cell loss occurred. These indicated that the underlying pathophysiological mechanisms of glaucoma are partially associated with the dysfunction of the cholinergic system in the visual pathway. Since citicoline undergoes a quick transformation to Cho and cytidine after administration and crosses the blood–brain barrier into the central nervous system, it is likely that a mechanism for citicoline to provide neuroprotective treatment to glaucoma is to normalize and replace the insufficient Cho contents in the glaucomatous visual cortex. ^{1}H MRS is a potential tool for studying the metabolic changes in glaucoma *in vivo* in normally appearing brain structures, and may possess direct clinical applications for humans. Measurement of the Cho:Cr reduction in the visual cortex can be a noninvasive biomarker for this disease.

Acknowledgments

The authors would like to thank Dr. Qing-ling Fu of the Department of Anatomy at The University of Hong Kong for her technical assistance. This work was supported in part by Hong Kong Research Grant Council and The University of Hong Kong CRCG grant.

References

Babb, S.M., Appelmans, K.E., Renshaw, P.F., Wurtman, R.J., Cohen, B.M., 1996. Differential effect of CDP-choline on brain cytosolic choline levels in younger and older subjects as measured by proton magnetic resonance spectroscopy. Psychopharmacology (Berl.) 127, 88–94.

Babb, S.M., Ke, Y., Lange, N., Kaufman, M.J., Renshaw, P.F., Cohen, B.M., 2004. Oral choline increases choline metabolites in human brain. Psychiatry Res. 130, 1–9.

Baughman, R.W., Gilbert, C.D., 1980. Aspartate and glutamate as possible neurotransmitters of cells in layer 6 of the visual cortex. Nature 287, 848–850.

Bianchi, M.C., Tosetti, M., Battini, R., Manca, M.L., Mancuso, M., Cioni, G., Canapicchi, R., Siciliano, G., 2003. Proton MR spectroscopy of mitochondrial diseases: analysis of brain metabolic abnormalities and their possible diagnostic relevance. AJNR (Am. J. Neuroradiol.) 24, 1958–1966.

Boucard, C.C., Hoogduin, J.M., van der Grond, J., Cornelissen, F.W., 2007. Occipital proton magnetic resonance spectroscopy (^{1}H-MRS) reveals normal metabolite concentrations in retinal visual field defects. PLoS ONE 2, e222.

Boucard, C.C., Mostert, J.P., Cornelissen, F.W., De Keyser, J., Oudkerk, M., Sijens, P.E., 2005. Visual stimulation, ^{1}H MR spectroscopy and fMRI of the human visual pathways. Eur. Radiol. 15, 47–52.

Boulanger, Y., Labelle, M., Khiat, A., 2000. Role of phospholipase A(2) on the variations of the choline signal intensity observed by ^{1}H magnetic resonance spectroscopy in brain diseases. Brain Res. Brain Res. Rev. 33, 380–389.

Carelli, V., Ross-Cisneros, F.N., Sadun, A.A., 2004. Mitochondrial dysfunction as a cause of optic neuropathies. Prog. Retin. Eye Res. 23, 53–89.

Chan, K.C., Fu, Q.L., Guo, H., So, K.F., Wu, E.X., 2008a. GD-DTPA enhanced MRI of ocular transport in a rat model of chronic glaucoma. Exp. Eye Res. 87, 334–341.

Chan, K.C., Fu, Q.L., Hui, E.S., So, K.F., Wu, E.X., 2008b. Evaluation of the retina and optic nerve in a rat model of chronic glaucoma using in vivo manganese-enhanced magnetic resonance imaging. NeuroImage 40, 1166–1174.

Chan, K.C., Fu, Q.L., So, K.F., Wu, E.X., 2007. Evaluation of the visual system in a rat model of chronic glaucoma using manganese-enhanced magnetic resonance imaging. Conf. Proc. IEEE Eng. Med. Biol. Soc. 2007, 67–70.

Collier, B., Mitchell, J.F., 1967. The central release of acetylcholine during consciousness and after brain lesions. J. Physiol. 188, 83–98.

Cordoba, J., Sanpedro, F., Alonso, J., Rovira, A., 2002. ^{1}H magnetic resonance in the study of hepatic encephalopathy in humans. Metab. Brain Dis. 17, 415–429.

Crawford, M.L., Harwerth, R.S., Smith 3rd, E.L., Shen, F., Carter-Dawson, L., 2000. Glaucoma in primates: cytochrome oxidase reactivity in parvo- and magnocellular pathways. Investig. Ophthalmol. Vis. Sci. 41, 1791–1802.

Cudalbu, C., Cavassila, S., Rabeson, H., van Ormondt, D., Graveron-Demilly, D., 2008. Influence of measured and simulated basis sets on metabolite concentration estimates. NMR Biomed. 21, 627–636.

Dowling, C., Bollen, A.W., Noworolski, S.M., McDermott, M.W., Barbaro, N.M., Day, M.R., Henry, R.G., Chang, S.M., Dillon, W.P., Nelson, S.J., Vigneron, D.B., 2001. Preoperative proton MR spectroscopic imaging of brain tumors: correlation with histopathologic analysis of resection specimens. AJNR (Am. J. Neuroradiol.) 22, 604–612.

Duncan, R.O., Sample, P.A., Weinreb, R.N., Bowd, C., Zangwill, L.M., 2007. Retinotopic organization of primary visual cortex in glaucoma: comparing fMRI measurements of cortical function with visual field loss. Prog. Retin. Eye Res. 26, 38–56.

Ende, G., Braus, D.F., Walter, S., Henn, F.A., 2001. Lower concentration of thalamic *n*-acetylaspartate in patients with schizophrenia: a replication study. Am. J. Psychiatry 158, 1314–1316.

Fleming, M.D., Benca, R.M., Behan, M., 2006. Retinal projections to the subcortical visual system in congenic albino and pigmented rats. Neuroscience 143, 895–904.
Fonnum, F., Lock, E.A., 2004. The contributions of excitotoxicity, glutathione depletion and DNA repair in chemically induced injury to neurones: exemplified with toxic effects on cerebellar granule cells. J. Neurochem. 88, 513–531.
Fournier, G.N., Semba, K., Rasmusson, D.D., 2004. Modality- and region-specific acetylcholine release in the rat neocortex. Neuroscience 126, 257–262.
Gatzioufas, Z., Charalambous, P., Seitz, B., Evers, S., Jonescu-Cuypers, C., Krause, M., Thanos, S., 2008. Cholinergic inhibition by botulinum toxin in a rat model of congenital glaucoma raises intraocular pressure. Br. J. Ophthalmol. 92, 826–831.
Gomez-Anson, B., Alegret, M., Munoz, E., Sainz, A., Monte, G.C., Tolosa, E., 2007. Decreased frontal choline and neuropsychological performance in preclinical Huntington disease. Neurology 68, 906–910.
Grieb, P., Rejdak, R., 2002. Pharmacodynamics of citicoline relevant to the treatment of glaucoma. J. Neurosci. Res. 67, 143–148.
Gruetter, R., 1993. Automatic, localized in vivo adjustment of all first- and second-order shim coils. Magn. Reson. Med. 29, 804–811.
Gu, Q., 2003. Contribution of acetylcholine to visual cortex plasticity. Neurobiol. Learn. Mem. 80, 291–301.
Gupta, N., Ang, L.C., Noel de Tilly, L., Bidaisee, L., Yucel, Y.H., 2006. Human glaucoma and neural degeneration in intracranial optic nerve, lateral geniculate nucleus, and visual cortex. Br. J. Ophthalmol. 90, 674–678.
Gupta, N., Yucel, Y.H., 2003. Brain changes in glaucoma. Eur. J. Ophthalmol. 13 (Suppl. 3), S32–S35.
Gupta, N., Yucel, Y.H., 2007. Should we treat the brain in glaucoma? Can. J. Ophthalmol. 42, 409–413.
Hui, E.S., Fu, Q.L., So, K.F., Wu, E.X., 2007. Diffusion tensor MR study of optic nerve degeneration in glaucoma. Conf. Proc. IEEE Eng. Med. Biol. Soc. 2007, 4312–4315.
Juchem, C., Logothetis, N.K., Pfeuffer, J., 2005. High-resolution (1)H chemical shift imaging in the monkey visual cortex. Magn. Reson. Med. 54, 1541–1546.
Kantarci, K., Weigand, S.D., Petersen, R.C., Boeve, B.F., Knopman, D.S., Gunter, J., Reyes, D., Shiung, M., O'Brien, P.C., Smith, G.E., Ivnik, R.J., Tangalos, E.G., Jack Jr., C.R., 2007. Longitudinal ^{1}H MRS changes in mild cognitive impairment and Alzheimer's disease. Neurobiol. Aging 28, 1330–1339.
Kaufman, P.L., 1999. Nitric-oxide synthase and neurodegeneration/neuroprotection. Proc. Natl. Acad. Sci. U.S.A. 96, 9455–9456.
Kim, Y.H., Pae, Y.S., Cho, B.C., 1995. The effect of unilateral orbital enucleation on acetylcholine and muscarinic receptors in visual pathway, and physical activity of rats. J. Korean Ophthalmol. Soc. 36, 855–867.
Lam, D.Y., Kaufman, P.L., Gabelt, B.T., To, E.C., Matsubara, J.A., 2003. Neurochemical correlates of cortical plasticity after unilateral elevated intraocular pressure in a primate model of glaucoma. Investig. Ophthalmol. Vis. Sci. 44, 2573–2581.
Laplante, F., Morin, Y., Quirion, R., Vaucher, E., 2005. Acetylcholine release is elicited in the visual cortex, but not in the prefrontal cortex, by patterned visual stimulation: a dual in vivo microdialysis study with functional correlates in the rat brain. Neuroscience 132, 501–510.
Li, R.S., Chen, B.Y., Tay, D.K., Chan, H.H., Pu, M.L., So, K.F., 2006a. Melanopsin-expressing retinal ganglion cells are more injury-resistant in a chronic ocular hypertension model. Investig. Ophthalmol. Vis. Sci. 47, 2951–2958.
Li, R.S., Tay, D.K., Chan, H.H., So, K.F., 2006b. Changes of retinal functions following the induction of ocular hypertension in rats using argon laser photocoagulation. Clin. Experiment. Ophthalmol. 34, 575–583.
McKinnon, S.J., 2003. Glaucoma: ocular Alzheimer's disease? Front. Biosci. 8, s1140–s1156.
Michel, V., Yuan, Z., Ramsubir, S., Bakovic, M., 2006. Choline transport for phospholipid synthesis. Exp. Biol. Med. (Maywood) 231, 490–504.
Miller, B.L., 1991. A review of chemical issues in ^{1}H NMR spectroscopy: *N*-acetyl-L-aspartate, creatine and choline. NMR Biomed. 4, 47–52.
Mlynarik, V., Kohler, I., Gambarota, G., Vaslin, A., Clarke, P.G., Gruetter, R., 2008. Quantitative proton spectroscopic imaging of the neurochemical profile in rat brain with microliter resolution at ultra-short echo times. Magn. Reson. Med. 59, 52–58.
Moore, C.M., Breeze, J.L., Gruber, S.A., Babb, S.M., Frederick, B.B., Villafuerte, R.A., Stoll, A.L., Hennen, J., Yurgelun-Todd, D.A., Cohen, B.M., Renshaw, P.F., 2000. Choline, myo-inositol and mood in bipolar disorder: a proton magnetic resonance spectroscopic imaging study of the anterior cingulate cortex. Bipolar Disord. 2, 207–216.
Moreno, M.C., Sande, P., Marcos, H.A., de Zavalia, N., Keller Sarmiento, M.I., Rosenstein, R.E., 2005. Effect of glaucoma on the retinal glutamate/glutamine cycle activity. FASEB J. 19, 1161–1162.
Osborne, N.N., Lascaratos, G., Bron, A.J., Chidlow, G., Wood, J.P., 2006. A hypothesis to suggest that light is a risk factor in glaucoma and the mitochondrial optic neuropathies. Br. J. Ophthalmol. 90, 237–241.
Oshitari, T., Fujimoto, N., Adachi-Usami, E., 2002. Citicoline has a protective effect on damaged retinal ganglion cells in mouse culture retina. NeuroReport 13, 2109–2111.
Parisi, V., 2001. Impaired visual function in glaucoma. Clin. Neurophysiol. 112, 351–358.
Parisi, V., 2005. Electrophysiological assessment of glaucomatous visual dysfunction during treatment with cytidine-5′-diphosphocholine (citicoline): a study of 8 years of follow-up. Doc. Ophthalmol. 110, 91–102.
Parisi, V., Manni, G., Centofanti, M., Gandolfi, S.A., Olzi, D., Bucci, M.G., 2001. Correlation between optical coherence tomography, pattern electroretinogram, and visual evoked potentials in open-angle glaucoma patients. Ophthalmology 108, 905–912.
Parisi, V., Manni, G., Colacino, G., Bucci, M.G., 1999. Cytidine-5′-diphosphocholine (citicoline) improves retinal and cortical responses in patients with glaucoma. Ophthalmology 106, 1126–1134.
Paxinos, G., Watson, C., 2007. The Rat Brain in Stereotaxic Coordinates, sixth ed. Elsevier, Amsterdam, Boston.
Quigley, H.A., Broman, A.T., 2006. The number of people with glaucoma worldwide in 2010 and 2020. Br. J. Ophthalmol. 90, 262–267.
Ratiney, H., Sdika, M., Coenradie, Y., Cavassila, S., van Ormondt, D., Graveron-Demilly, D., 2005. Time-domain semi-parametric estimation based on a metabolite basis set. NMR Biomed. 18, 1–13.
Rejdak, R., Toczolowski, J., Kurkowski, J., Kaminski, M.L., Rejdak, K., Stelmasiak, Z., Grieb, P., 2003. Oral citicoline treatment improves visual pathway function in glaucoma. Med. Sci. Monit. 9, PI24–PI28.
Rothe, T., Hanisch, U.K., Krohn, K., Schliebs, R., Hartig, W., Webster, H.H., Biesold, D., 1990. Changes in choline acetyltransferase activity and high-affinity choline uptake, but not in acetylcholinesterase activity and muscarinic cholinergic receptors, in rat somatosensory cortex after sciatic nerve injury. Somatosens. Mot. Res. 7, 435–446.
Satlin, A., Bodick, N., Offen, W.W., Renshaw, P.F., 1997. Brain proton magnetic resonance spectroscopy (^{1}H-MRS) in Alzheimer's disease: changes after treatment with xanomeline, an M1 selective cholinergic agonist. Am. J. Psychiatry 154, 1459–1461.
Sato, H., Hata, Y., Hagihara, K., Tsumoto, T., 1987. Effects of cholinergic depletion on neuron activities in the cat visual cortex. J. Neurophysiol. 58, 781–794.
Schmidt, B.M., Rylett, R.J., 1993. Phosphorylation of rat brain choline acetyltransferase and its relationship to enzyme activity. J. Neurochem. 61, 1774–1781.
Secades, J.J., Lorenzo, J.L., 2006. Citicoline: pharmacological and clinical review, 2006 update. Methods Find. Exp. Clin. Pharmacol. 28 (Suppl. B), 1–56.
Smith, R., Chung, H., Rundquist, S., Maat-Schieman, M.L., Colgan, L., Englund, E., Liu, Y.J., Roos, R.A., Faull, R.L., Brundin, P., Li, J.Y., 2006. Cholinergic neuronal defect without cell loss in Huntington's disease. Hum. Mol. Genet. 15, 3119–3131.
Taylor-Robinson, S.D., Sargentoni, J., Marcus, C.D., Morgan, M.Y., Bryant, D.J., 1994. Regional variations in cerebral proton spectroscopy in patients with chronic hepatic encephalopathy. Metab. Brain Dis. 9, 347–359.
Thanos, S., Naskar, R., 2004. Correlation between retinal ganglion cell death and chronically developing inherited glaucoma in a new rat mutant. Exp. Eye Res. 79, 119–129.
Vetter, J.M., Jehle, T., Heinemeyer, J., Franz, P., Behrens, P.F., Jackisch, R., Landwehrmeyer, G.B., Feuerstein, T.J., 2003. Mice transgenic for exon 1 of Huntington's disease: properties of cholinergic and dopaminergic pre-synaptic function in the striatum. J. Neurochem. 85, 1054–1063.
Wang, X.C., Du, X.X., Tian, Q., Wang, J.Z., 2008. Correlation between choline signal intensity and acetylcholine level in different brain regions of rat. Neurochem. Res. 33, 814–819.
Weber, A., Harman, C.D., Viswanathan, S., 2008. Effects of optic nerve injury, glaucoma, and neuroprotection on the survival, structure, and function of ganglion cells in the mammalian retina. J. Physiol..
Wessler, I., Kilbinger, H., Bittinger, F., Unger, R., Kirkpatrick, C.J., 2003. The non-neuronal cholinergic system in humans: expression, function and pathophysiology. Life Sci. 72, 2055–2061.
Xu, S., Yang, J., Li, C.Q., Zhu, W., Shen, J., 2005. Metabolic alterations in focally activated primary somatosensory cortex of alpha-chloralose-anesthetized rats measured by ^{1}H MRS at 11.7 T. NeuroImage 28, 401–409.
Yasuhara, O., Tooyama, I., Aimi, Y., Bellier, J.P., Hisano, T., Matsuo, A., Park, M., Kimura, H., 2003. Demonstration of cholinergic ganglion cells in rat retina: expression of an alternative splice variant of choline acetyltransferase. J. Neurosci. 23, 2872–2881.
Yen, C.L., Mar, M.H., Zeisel, S.H., 1999. Choline deficiency-induced apoptosis in PC12 cells is associated with diminished membrane phosphatidylcholine and sphingomyelin, accumulation of ceramide and diacylglycerol, and activation of a caspase. FASEB J. 13, 135–142.
Yucel, Y.H., Zhang, Q., Weinreb, R.N., Kaufman, P.L., Gupta, N., 2003. Effects of retinal ganglion cell loss on magno-, parvo-, koniocellular pathways in the lateral geniculate nucleus and visual cortex in glaucoma. Prog. Retin. Eye Res. 22, 465–481.

ELSEVIER

NeuroImage

www.elsevier.com/locate/ynimg
NeuroImage 40 (2008) 1166–1174

Evaluation of the retina and optic nerve in a rat model of chronic glaucoma using in vivo manganese-enhanced magnetic resonance imaging

Kevin C. Chan,[a,b] Qing-ling Fu,[c] Edward S. Hui,[a,b] Kwok-fai So,[c] and Ed X. Wu[a,b,*]

[a]*Laboratory of Biomedical Imaging and Signal Processing, The University of Hong Kong, Hong Kong*
[b]*Department of Electrical and Electronic Engineering, The University of Hong Kong, Hong Kong*
[c]*Department of Anatomy, The University of Hong Kong, Hong Kong*

Received 19 July 2007; revised 21 December 2007; accepted 5 January 2008
Available online 17 January 2008

Glaucoma is a neurodegenerative disease of the visual system. While elevated intraocular pressure is considered to be a major risk factor, the primary cause and pathogenesis of the disease are still unclear. This study aims to employ in vivo manganese-enhanced magnetic resonance imaging (MEMRI) to evaluate dynamically the Mn^{2+} enhancements in the visual components following an induction of ocular hypertension in a rat model of chronic glaucoma. The episcleral and limbal veins were photocoagulated unilaterally in the right eye using an argon laser to maintain a consistent elevation of intraocular pressure by about 1.6 times above the normal level. Two and six weeks after glaucoma induction, $MnCl_2$ solution (50 mM, 3 μL) was injected intravitreally into both eyes, and MEMRI was performed 2 to 5 h after injection. Results showed a delayed increase in T1-weighted signal intensity in the glaucomatous optic nerve at 6 weeks but not 2 weeks after glaucoma induction. In addition, there was an accumulation of Mn^{2+} ions in the vitreous humour of the glaucomatous eye, with a high concentration of Mn^{2+} ions at the optic nerve head and the retina. These MEMRI findings may help understand the disease mechanisms, monitor the effect of drug interventions in glaucoma models and complement the conventional techniques in examining the glaucomatous visual components.

Keywords: Chronic glaucoma; Rat; Intraocular pressure; Optic nerve; Fast axonal transport; Manganese-enhanced magnetic resonance imaging

Introduction

Glaucoma is a neurodegenerative disease of the visual system characterized by retinal ganglion cell (RGC) death, optic nerve head (ONH) damage and progressive visual field loss (Thanos and Naskar, 2004). It is the second major cause of blindness in the world (Quigley and Broman, 2006). While elevated intraocular pressure (IOP) is considered to be a major risk factor, the primary cause to the disease mechanisms is still unclear (Kaufman, 1999; Morrison et al., 2005). Quantitative assessments of optic nerve (ON) axonal loss or brain changes in experimental models of glaucoma are typically performed postmortem in histological tissue sections (Lindsey et al., 2007; Morrison, 2005) or by electrophysiological techniques (Li et al., 2006a). However, these methods either fail to provide a global view of the brain or do not allow repeated measures for longitudinal studies (van der Linden et al., 2004). To understand the exact mechanisms of glaucomatous changes, there is a need to develop a novel, in vivo and three-dimensional method to investigate into the integrity of the primary visual system longitudinally.

Magnetic resonance imaging (MRI) provides a non-invasive tool to study the structural, metabolic and functional details of the inner depth of the body in vivo. Among the MRI techniques, diffusion tensor imaging has successfully detected and differentiated structurally the axon and myelin degeneration upon an evolving white matter injury in the mouse ON after retinal ischemia (Song et al., 2003; Sun et al., 2006). It has also been shown that the lamina-specific structures and functional responses in the retina can be resolved using Gd-DTPA contrast-enhanced MRI and high-resolution functional MRI (Cheng et al., 2006). Recently, manganese-enhanced magnetic resonance imaging (MEMRI) has been increasingly used to study both structural and functional changes in the central nervous system without reliance on hemodynamic response. It has been used to enhance the contrast in studies of neuroarchitecture (Aoki et al., 2004a), to trace neuronal pathways (Pautler, 2004; Paulter et al., 1998), to detect activated regions in the brain (Silva et al., 2004) and to investigate cerebral ischemic injury (Aoki et al., 2004b; Yang and Wu, 2008). Mn^{2+} ions are paramagnetic in nature and can shorten the T_1 relaxation time of the surrounding water protons. They act as a calcium analogue and enter the

* Corresponding author. Laboratory of Biomedical Imaging and Signal Processing, Department of Electrical and Electronic Engineering, The University of Hong Kong, Hong Kong. Fax: +852 2819 9711.
E-mail address: ewu@eee.hku.hk (E.X. Wu).
Available online on ScienceDirect (www.sciencedirect.com).

1053-8119/$ - see front matter © 2008 Elsevier Inc. All rights reserved.
doi:10.1016/j.neuroimage.2008.01.002

intracellular space via L-type voltage-gated calcium channels upon neuronal activation (Pautler, 2006). A fraction of the ions is then sequestered in the endoplasmic reticulum or Golgi apparatus and actively transported along the microtubules via fast axonal transport (Pautler, 2004; Van der Linden et al., 2007; Watanabe et al., 2004). On the other hand, a recent study has demonstrated the independence of electrical activity to Mn^{2+} uptake in the eye (Bearer et al., 2007), suggestive of alternative channels, e.g. divalent metal transporters (Takeda, 2003) for Mn^{2+} transport. Glial uptake and diffusion may also contribute to the cerebral pattern in Mn^{2+} enhancement (Watanabe et al., 2004). In the current study, we aimed to examine the Mn^{2+} transport in the normal and glaucomatous eyes upon intravitreal injection and to correlate the in vivo results with previous histological findings. These may help optimize the investigation into the integrity of the visual system and the possibility of ocular drug delivery into the glaucomatous eyes.

MEMRI has been used to examine the axonal transport of the central nervous system in rodents. As Mn^{2+} can access the nervous system intraaxonally without the reliance on hemodynamic response, studies evaluated the axonal transport rate in Alzheimer's disease (Smith et al., 2007) and diabetes (Serrano et al., 2007) and upon drug treatment (Smith et al., 2007). On the other hand, axon degeneration has been demonstrated by the blockade of Mn^{2+} transport at sites of radiation-induced injury (Ryu et al., 2002) and ON crush (Thuen et al., 2005) upon intravitreal injection. By applying MEMRI, it is also possible to compare the cross-sectional areas in the prechiasmatic regions of the ON induced with optic glioma (Banerjee et al., 2007). In the experimental rat model of chronic glaucoma in our laboratory, chronic IOP elevation induces a 3% RGC loss per week across the 8-week experimental period (Li et al., 2006a). Other reports indicated an early damage from an elevated IOP in the superior regions of the rat ON (Morrison, 2005, Quigley et al., 1987; Wang et al., 2004), while atrophy of large fibers was observed in areas of the ON with mild damage (Johnson et al., 2000; Quigley et al., 1987). It was also suggested that the axoplasmic flow happened to be disturbed upon chronic IOP elevation (Dandona et al., 1991; Johnson et al., 2000; Khosla et al., 1982). In experimental mouse ocular hypertension, the ON mean axon density and total number of axons in the laser-treated eyes were found to be significantly less than in the control eyes (Mabuchi et al., 2003; Mabuchi et al., 2004). Therefore, we hypothesize that there would be a reduction in Mn^{2+} transport along the glaucomatous ON, especially in the superior regions.

Further, previous studies using high-resolution MEMRI detected layer-specific retinal functional adaptation (Berkowitz et al., 2006), as well as changes in intraretinal signal intensities in rat models of ON injury and choroidal melanoma (Berkowitz et al., 2007; Braun et al., 2007). In addition to the RGC loss, it was shown that ocular hypertension appeared to accompany with ischemia, axonal swelling and mechanical alteration of the laminar layers at the ONH (Gross et al., 2003; Kaufman, 1999). To account for these, we would attempt to test if there would be signal changes in the retina and the ONH between the glaucomatous and the control eyes.

Lastly, Mn^{2+} has been applied trans-sclerally, transcorneally and intravitreally to evaluate its distribution in the eyeballs for ocular drug delivery (Li et al., 2004; Molokhia et al., 2007). The glaucoma model in the current study involves laser photocoagulation of the episcleral and limbal veins, which contributes to the obstruction of venous outflow in rats (Li et al., 2006a; Morrison et al., 1995). Blockade of this drainage would induce a 1.6-fold increase in IOP (Chan et al., 2007; Fu et al., 2007; Li et al., 2006a,b). By employing dynamic MEMRI, we hypothesize that the usual pattern of Mn^{2+} clearance in the glaucomatous eyeball will be perturbed upon intravitreal injection.

To our knowledge, this is the first attempt to apply dynamic MEMRI to investigate the chronic glaucoma within the rat primary visual system in vivo. This is particularly valuable as we may be able to apply MEMRI to understand the disease mechanisms and resolve the functional loss and recovery of neuronal connectivity (van der Zijden et al., 2007) upon drug treatment (Chan et al., 2007; Fu et al., 2007).

Methods

Animal preparation

Sprague–Dawley female rats (250–280 g, 3 months old, $N=15$) were reared in a temperature-controlled room subjected to a 12-h light/12-h dark cycle with standard chow and water supply ad libitum. They were divided into 3 groups (see Fig. 1). Except for the control group, the rats were induced for ocular hypertension unilaterally in the right eye by photocoagulation of the episcleral and limbal veins using an argon laser. A second laser treatment in the same settings was applied 7 days later to block the neovascular flow and maintain a consistent IOP elevation by about 1.6 times above the normal level. This technique was adopted from the method by WoldeMussie et al (2001) and has been adopted in our laboratory with track record of recent publications (Chan et al., 2007; Fu et al., 2007; Li et al., 2006a,b). The IOPs of the glaucomatous and control eyes were measured using a calibrated tonometer (Tonopen-XL, Mentor, Norwell, MA, USA) and were found to be 15.01 ± 0.50 mmHg and 14.00 ± 1.02 mmHg, respectively, before laser treatments ($p=0.41$) and 24.78 ± 0.88 mmHg and 15.21 ± 0.30 mmHg, respectively, after two laser treatments ($p<0.01$). After the rats were anaesthetized with an intraperitoneal injection of a mixture of ketamine (70 mg/kg) and xylazine (7 mg/kg), $MnCl_2$ solution (50 mM, 3 μL, diluted with Milli-Q-H_2O) was injected intravitreally into both eyes using a 10-μl Hamilton microsyringe fixed with a 26-s gauge needle (Hamilton, catalog #80300). The microsyringe was held inside the eyeball for more than 1 minute before being pulled out. The rats were then returned to the cage and were laid prone under a warm lamp until their recovery. Given a recent finding of a permanent loss of 10–20% of the axons in the normal mouse ON even after a single injection of a lower amount of $MnCl_2$ (Bearer et al., 2007), the Mn^{2+} solution was injected into two separate groups at 2 weeks (Group 1, $n=6$) and 6 weeks (Group 2, $n=6$) after starting the glaucoma induction, so as to minimize Mn^{2+} toxicity to the neurons, and injuries to the eyeball from multiple injections, and to eliminate the possibility of MRI signal reduction resulting from repeated injections (Thuen et al., 2005) rather than from the disease progression in the same animal.

MRI protocols

All MRI measurements were acquired on a 7-T MRI scanner with a maximum gradient of 360 mT/m (70/16 PharmaScan, Bruker Biospin GmbH, Germany) using a 38-mm rat brain quadrature resonator for RF transmission and receiving. Rats were placed onto a head holder consisting of ear and tooth bars. Since the rate of axonal transport varies with temperature (Smith et al., 2007), under inhaled isoflurane anesthesia (2% induction and 1% maintenance), animals were kept warm on a heating pad circulated with water at 37 °C. Two syringe phantoms containing 0.05 mM of $MnCl_2$ solution were

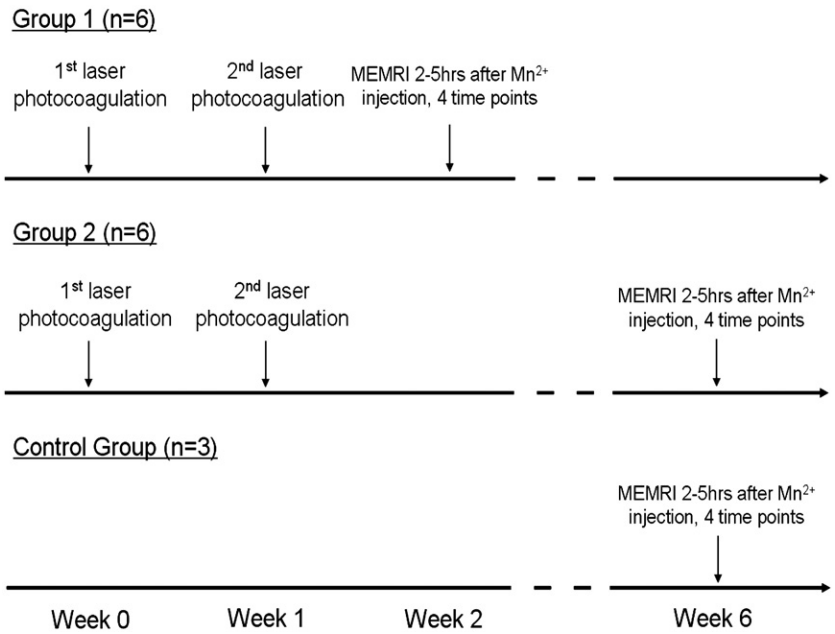

Fig. 1. Schedule of the 1st and 2nd laser treatments (1 week apart) for induction of chronic glaucoma, intravitreal Mn^{2+} injection and T1-weighted MEMRI. MEMRI was performed 2 weeks after the 1st laser treatment for Group 1 ($n=6$) and 6 weeks after 1st laser treatment for Group 2 ($n=6$). No laser treatment was performed in the control group. Note that Mn^{2+} was administered only once in all animals.

inserted beside the rat for signal intensity normalization during post-processing. Dynamic MEMRI was performed 2 to 5 h after Mn^{2+} injection in order to capture the early arrival of Mn^{2+} ions along the ONs (see Fig. 1). Throughout the experiments, the left eye served as a control. Three-dimensional volumetric images were acquired using an isotropic T1-weighted 3D RARE sequence with fat suppression, TR/TE = 300/6.6 ms, RARE factor = 4, NEX = 2, FOV = $3.24 \times 3.24 \times 2.47$ cm^3 and voxel resolution = $193 \times 193 \times 193$ μm^3. The 3D slab was positioned to parallel the prechiasmatic ONs based on the axial, coronal and sagittal multi-slice T2-weighted RARE images acquired with TR/TE = 4200/36 ms, RARE factor = 8, NEX = 1, FOV = 4×4 cm^2, pixel resolution = 156×156 μm^3, slice thickness = 0.7 mm and number of slices = 18. The acquisition time for each 3D T1-weighted image set was 40 minutes. Images at 4 time points (i.e. 140, 180, 220 and 260 min after Mn^{2+} injection) were acquired for each animal.

Data analysis

All 3D images were co-registered using AIR v5.2.5 (Roger Woods, UCLA, USA). The MEMRI signal intensities in the prechiasmatic left and right ONs were measured with an identical volume-of-interest (VOI) ($2 \times 2 \times 6$ voxels) placed at about 1.5 mm anterior to the optic chiasm at all time points using BrainSuite v2.0 (LONI, UCLA, USA) to monitor the Mn^{2+} transport along the ONs (see Fig. 2). In order to evaluate the Mn^{2+} transport and to weight out the effect of possible dosage difference applied to both eyes, the values at the prechiasmatic ONs were normalized to those at the first time point (i.e. 140 min after Mn^{2+} injection). In the reconstructed 2D slice that centrally cut through the eyeball and ONH, regions of interest (ROIs) were also drawn manually on the vitreous humour and the retina, covering a distance of 2.5 mm on each side from the ONH using ImageJ v1.37 (Wayne Rasband, NIH, USA). The signal intensities at 260 min after Mn^{2+} injection were analyzed by taking their mean values. Each value was normalized to the nearby syringe phantom to avoid the effect of any system sensitivity drift. Differences between mean values of the ROIs on both sides were compared using two-tailed paired *t*-tests, and the mean values along the time course were compared using ANOVA. Results were considered to be significantly different when $p<0.05$. During the analyses, the data sets were blinded by flipping the images left-right

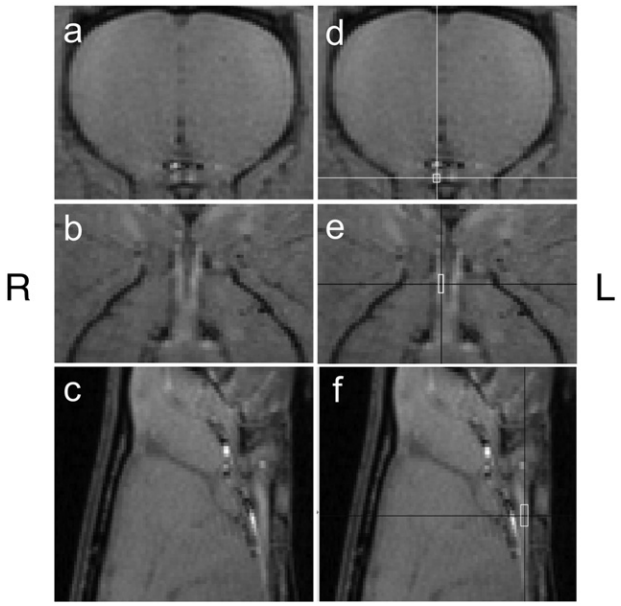

Fig. 2. Localization of the volume of interest (VOI, $2 \times 2 \times 6$ voxels) onto the Mn-enhanced prechiasmatic optic nerve in the coronal (a, d), axial (b, e) and sagittal (c, f) views of the same animal. The 3D image slab was positioned to parallel with the prechiasmatic optic nerves. (a–c) T1-weighted raw images; (d–f) same images with VOI overlay.

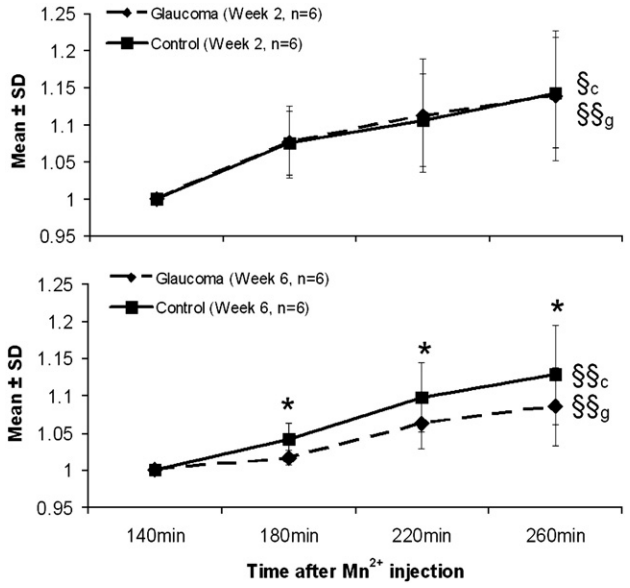

Fig. 3. Time course of T1-weighted signal intensities (normalized to those at the first time point) at the prechiasmatic optic nerve VOI in Week 2 animals (Group 1, top) and Week 6 animals (Group 2, bottom). Significant signal increase was observed in both sides of the prechiasmatic optic nerves of all animals over time (ANOVA across timeline in glaucomatous (g) and control (c) optic nerves with $^{\S}p<0.05$ and $^{\S\S}p<0.01$). Reduction of Mn^{2+} transport in the glaucomatous (right) optic nerve was observed in the Week 6 animals but not in the Week 2 ones by two-tailed paired *t*-tests with $*p<0.05$. Two-tailed unpaired *t*-tests gave no significant differences in the control optic nerves between Week 2 and Week 6 models at all time points ($p>0.05$).

randomly and the ROIs were drawn without realizing the actual left and right positions.

Histological analysis of the optic nerve

Given that our study was based upon the early arrival of Mn^{2+} ions, to rule out the effect of Mn^{2+} toxicity aforementioned to the histological results, a separate group of animals ($n=4$) were induced with chronic glaucoma and were euthanized with a lethal intravenous injection of sodium pentobarbital (1 mg/kg) 6 weeks after glaucoma induction. Segments of the prechiasmatic ON containing the VOIs analyzed in MEMRI were excised and fixed by immersing in 2.5% glutaraldehyde and 2% paraformaldehyde in PBS for at least 1 week at 4 °C after each ON was enucleated. After three washes with PBS, the ON segments were placed in 2% osmium tetroxide in saline for 2 h and washed with PBS at room temperature. Subsequently, they were dehydrated in alcohol and embedded in epoxy resin for sectioning. Cross sections of 1 μm thickness were cut on an ultra-microtome, mounted on glass slides and stained for myelin using 0.5% toluidine blue (Sasaoka et al., 2006). The axonal density was measured using a microscopic analysis system (Optiphot Fluorescence Microscope, Nikon Instruments Inc., NY) in a meshed fashion. Briefly, each ON cross section slide was divided into approximately ten 150×150 μm^2 counting frames. Axons within a 30×30 μm^2 sample area in each counting frame were counted at 40× magnification, representing approximately 4% of the total ON cross-sectional area. The numbers of the axons counted in the sampling areas of each ON were then averaged to compute the axonal density. Three slides were quantified per ON, whereas each estimate was based on counts of between 1500 and 2500 axons. Axonal density measurements were compared between glaucomatous and contralateral ONs using one-tailed paired *t*-tests.

Table 1
Ratios of T1-weighted signal intensities (SI) between glaucomatous and contralateral eyes 260 min after Mn^{2+} injection

Ratios of SI between glaucomatous and contralateral eyes	Retina (paired *t*-test between glaucomatous and contralateral eyes)	Vitreous humour (paired *t*-test between glaucomatous and contralateral eyes)
Control group ($n=3$)	0.99 ± 0.03 ($p=0.67$)	0.99 ± 0.09 ($p=0.65$)
Group 1 ($n=6$)	1.22 ± 0.11 ($*p=0.006$)	0.96 ± 0.05 ($p=0.09$)
Group 2 ($n=6$)	1.09 ± 0.05 ($*p=0.005$)	1.24 ± 0.16 ($*p=0.02$)
ANOVA among 3 groups	$*p=0.03$	$*p=0.005$

Results

Mn^{2+} transport in prechiasmatic optic nerve

Fig. 2 illustrates the placement of the VOI in one of the prechiasmatic ONs. As shown in Fig. 3, MEMRI signal increased significantly in both sides of the prechiasmatic ONs of all animals over time after Mn^{2+} injection (ANOVA: $p<0.05$). A reduction in the Mn^{2+} transport was observed at the prechiasmatic region of the

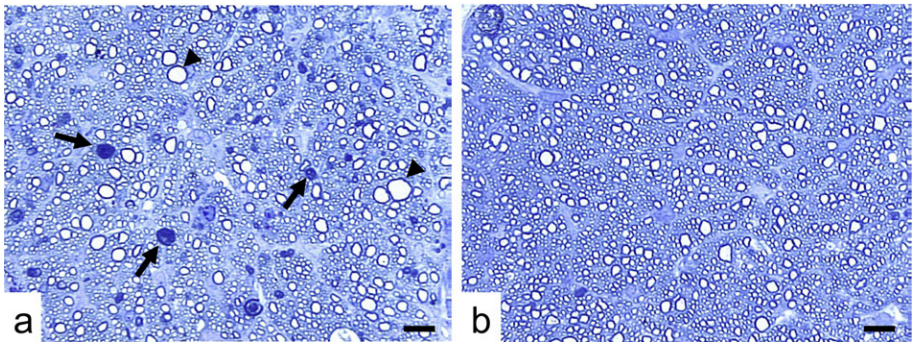

Fig. 4. Light micrograph of the prechiasmatic optic nerves (ONs) in the glaucomatous (a) and normal (b) eyes 6 weeks after glaucoma induction (toluidine blue stain, 40× magnification). In the glaucomatous ON, degenerating axons appear swollen (arrowheads) or dark due to collapsed myelin sheaths (arrows); whereas in the control ON, the staining looked more homogeneous. Axons were uniform in shape and packed together tightly to form the fibers of the nerve. Scale bar, 10 μm. (For interpretation of the references to colour in this figure legend, the reader is referred to the web version of this article.)

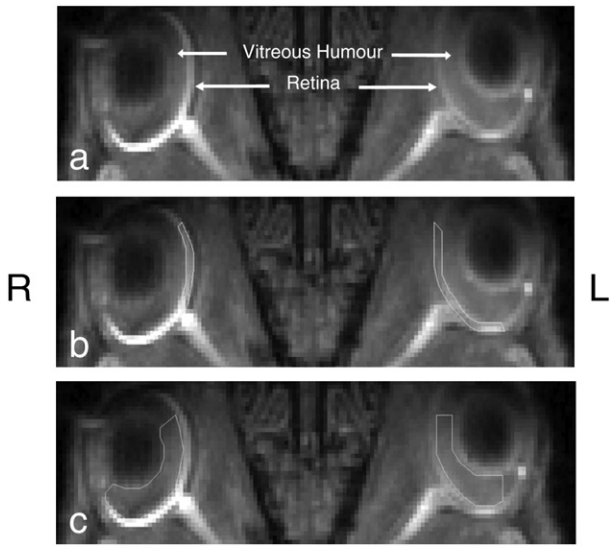

Fig. 5. Typical ROI delineations for the analysis of retina (mid row) and vitreous humour (bottom row) in the T1-weighted image of a rat from Group 1 (2 weeks after 1st laser treatment). Mean signal intensities in both retina and vitreous humour were obtained covering a distance of 2.5 mm on each side from the optic nerve head at 260 min after Mn^{2+} injection.

glaucomatous ON compared to the contralateral side in the Week 6 model in Group 1, while there was no apparent reduction in the Mn^{2+} transport in the Week 2 model in Group 2. Two-tailed unpaired *t*-tests gave no significant differences in the control ONs between Week 2 and Week 6 models at all time points ($p > 0.05$).

Fig. 4 shows a representative pair of glaucomatous and control ONs upon toluidine blue staining at 6 weeks after glaucoma induction. In the glaucomatous ON, degenerating axons appear swollen or dark due to collapsed myelin sheaths; whereas in the control ON, the staining looked more homogeneous. The average axonal densities in the glaucomatous and control ONs were estimated to be 0.18 ± 0.03 and 0.20 ± 0.02 axons/μm^2, respectively, contributing to an approximation of 10% loss in the glaucomatous ON ($p < 0.05$). It was suspected that many optic nerve axons in the rat are smaller than the practical limits of their resolution by light microscopy (LM) (Chauhan et al., 2006; Morrison et al., 2005). However, given that the large fibers were more vulnerable to atrophy in areas of the ON with mild glaucomatous damage (Johnson et al., 2000; Quigley et al., 1987), these fibers should practically be distinguishable by our LM analyses as shown in Fig. 4, leading to the distinct differences in our LM measurements between contralateral ONs. We have also estimated a smaller number of ON sections with the addition of a 100× oil-immersion objective, and the axonal density was found to be about 0.5 axons/μm^2, which was similar to the literature value for the intracranial ON in the same strain and gender using electron microscopy (0.4876 ± 0.0461 axons/μm^2) (Lau et al., 2006). Although the use of the 100× oil-immersion objective would have allowed resolution of finer detail and application of criteria even closer to those used for counting axons with EM (Chauhan et al., 2006), we had minimized the additional work required for such method as our purpose of performing histology at the prechiasmatic optic nerve was primarily to confirm the validity and consistency of our model.

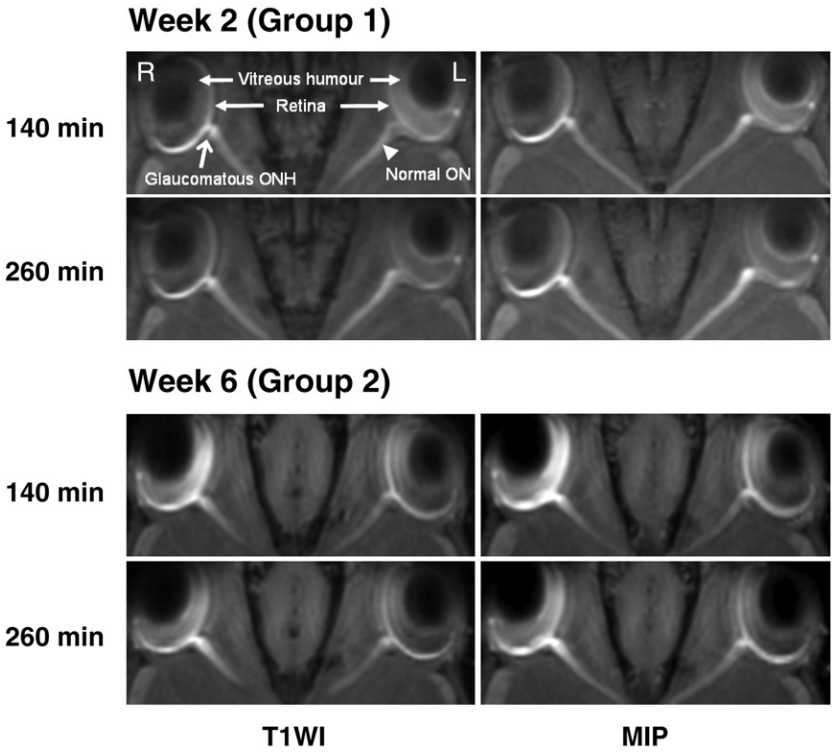

Fig. 6. Typical T1-weighted images (T1WI) of the glaucoma model (1st column) and targeted maximum intensity projection (MIP) of the optic nerves (2nd column). Accumulation of Mn^{2+} ions at high concentrations was clearly observed at the glaucomatous optic nerve head (ONH) (open arrow) compared to the normal ONH in Week 2 (Group 1, top 2 rows) and Week 6 (Group 2, bottom 2 rows) animals. Significantly higher signal intensity in the vitreous humour of the glaucomatous eye was also found at 6 weeks after 1st laser treatment. Note that the images shown were acquired 140 min and 260 min after Mn^{2+} injection.

Retina and optic nerve head

The retinal signal intensities were significantly higher in the glaucomatous eyes than in the contralateral eyes in both Week 2 and Week 6 animals as indicated in Table 1. Fig. 5 illustrates the ROI delineation for retinal and vitreous humour analysis. The typical Mn^{2+} enhancement of eye and ON structure was shown in Fig. 6. An apparent accumulation of Mn^{2+} ions at high concentrations was observed in the ONH, with more being observed in the glaucomatous eye in Group 1 (5 out 6 animals) and Group 2 (3 out of 6 animals) as indicated in the arrows in Fig. 6.

Time profile in vitreous humour

Signal intensities (SI) in the vitreous humour of both eyes decreased as time progressed for all groups after Mn^{2+} injection (data not shown). At 260 min after Mn^{2+} injection, the vitreous humour in the glaucomatous eye had a significantly higher signal intensity than that in the contralateral side in all Week 6 animals as shown in Table 1 ($p<0.05$) and illustrated in Fig. 6 and in 2 out of 6 of the Week 2 animals ($p=0.09$) but not in the control group ($p>0.05$).

Discussion and conclusion

Mn^{2+} transport along the optic nerve

Mn^{2+} ions have been verified to be uptaken by the RGCs, packed into organelles in the endoplasmic reticulum and transported along microtubules in the ONs (Pautler, 2006; Van der Linden et al., 2007). The rate of signal accumulation at a target location would be expected to depend on the uptake rate of Mn^{2+} at the injection site, the density of projections and the transport and/or diffusion away from the target location (Leergaard et al., 2003). In the current study, Mn^{2+} enhancement in ONs was seen to increase as early as at 180 min after injection. Given the length of the normal rat ON from ONH to the optic chiasm to be 10.55±0.70 mm for the 15 samples in our study, the Mn^{2+} transport at the prechiasmatic ONs at about 1.5 mm anterior to optic chiasm should rate at approximately 3.02 mm/h, which is within the range of fast axonal transport of 2 to 16 mm/h (Elluru et al., 1995) and is consistent with reported values in previous studies along the ONs (5 mm/h, Bearer et al., 2007; 2 mm/h, Pautler et al., 1998; 2.8 mm/h, Watanabe et al., 2001).

The apparent reduction in the rate of Mn^{2+} transport (or, more precisely, the Mn^{2+} enhancement increase) in the prechiasmatic ON of the glaucomatous eye in the Week 6 model may arise from several factors that comprise its transport route. Firstly, the RGC loss in this experimental model of chronic glaucoma ranges from 22% to 25% at 4 to 8 weeks after 1st laser treatment (Li et al., 2006a). This could cause a reduction in Mn^{2+} uptake into the RGCs, and thus a reduction in the overall anterograde transport in the axons of the retinal nerve fiber layer; secondly, our current findings have also demonstrated a significant reduction in average axonal densities at the prechiasmatic ON using toluidine blue staining. This appears to correlate with the mean axonal density decrease in other chronic glaucoma studies (Mabuchi et al., 2003; Mabuchi et al., 2004; Sasaoka et al., 2006) despite their interstrain variations (Hetling et al., 2005; Lau et al., 2006) and different microscopic methods used (Chauhan et al., 2006; Morrison, et al., 2005). The decrease in ON axonal density may reduce the amount of Mn^{2+} ions transported along the ON bundles per unit time as it was observed in the current experiment. Note that the cross-sectional area in the control ON (228221±27931 μm^2) was similar to the literature value determined by electron microscopy (230284±41122 μm^2) (Lau et al., 2006), while the areas of the glaucomatous ONs in our glaucoma model were not statistically significant from those of the control ONs ($p=0.18$). Thirdly, there might be a blockade in axoplasmic transport along the glaucomatous ON. It has been reported that the fast axonal transport was obstructed at the glaucomatous ON by studying the movement of radioactive materials (Anderson and Hendrickson, 1974; Dandona et al., 1991; Quigley et al., 1979; Quigley and Addicks, 1980). Our histological findings have also shown swollen and enlarged ONs in agreement with a previous study of similar period of IOP elevation (39 days at 27±9 mmHg; Johnson et al., 2000). When visualized in electron microscopy, these ONs were usually characterized by accumulation of organelles, vesicles and dense bodies especially in the large diameter axons, indicative of blocked axonal transport (Grozdanic et al., 2003; Johnson et al., 2000; Morrison et al., 1997; Quigley et al., 1987). As the number of microtubules was found to increase with axonal size in the ONs of adult rats (Hernandez et al, 1989), it is likely that the delay in T1-weighted signal increase in our findings could reflect damages to the microtubules particularly in the large fibers; In addition, abnormal processing of amyloid precursor protein (APP) has once been observed in rat glaucoma (Vickers et al., 2002). Amyloid-beta (Aβ) plaques resulting from the sequential cleavage of the APP were shown to rapidly inhibit fast axonal transport in cultured rat hippocampal neurons (Hiruma et al., 2003). Given that a previous MEMRI study has shown the decrease in fast axonal transport in Alzheimer's disease after Aβ deposition in the olfactory system (Smith et al., 2007), it is possible that the same would occur along the visual pathways of the glaucoma models as well. It is also possible that the changes in manganese concentration in the vitreous humour might affect the signal increase in the prechiasmatic optic nerve of both eyes. However, a comprehensive model that might describe the input function, the mechanisms of active Mn^{2+} transport in the visual components and the diffusion pattern along the optic nerve is still lacking, while T1 mapping has not been carried out to quantify the Mn^{2+} concentrations in the visual components. Thus, it is inherently difficult to analyze the rate of axonal transport in the optic nerve precisely from one segment to another in the current study.

The delayed T1-weighted signal increase was found to be significant only in the Week 6 model but not in the Week 2 one. In addition, a preliminary study on 2 Week 9 animals by the same setup has also shown an apparent reduction in Mn^{2+} signal increase as the Week 6 animals did (data not shown). These appeared to suggest the disease progression along the time course. The glaucoma model in the current study was proven to induce a chronic disease with an RGC loss of 12–14% at 2 weeks after induction (Fu et al., 2007; Li et al., 2006a), which was approximately half of that at 4 to 8 weeks after induction. Note also that histological analysis on the progression of ON damage using toluidine blue staining has been documented previously for a chronic glaucoma model, revealing a significant reduction of axonal density at Week 8 but not Week 4 or earlier after glaucoma induction (Sasaoka et al., 2006). The glaucomatous changes along the ONs in the early stage might not be detectable by MEMRI used in the current study.

Retinal enhancement and optic nerve head occlusion

Despite the proven RGC loss which might reduce the overall signal intensity of the retina, The significance of the increase in the

signal intensities of the retina measured in the glaucomatous eyes when compared to the contralateral ones remains unclear. One potential explanation could be related to the competing effect of increased reactive gliosis (WoldeMussie et al., 2001) and microglial activation (Naskar et al., 2002) on the retina, which might take up the Mn^{2+} ions concurrently (Kawai et al., 2007; Haapanen et al., 2007). Mn^{2+} might also be trapped in the retinal nerve fiber layer due to the blockade at the ONH and the ON. While some investigators have observed changes in the glaucomatous outer retina in clinical-histopathologic studies (Morrison et al., 2005), it has also been postulated that, when the intraocular pressure was increased by a tumor-induced change, outer retinal ion demand might be raised and the retinal signal intensities would increase further upon intraperitoneal Mn^{2+} injection (Braun et al., 2007). Note that alterations of intraretinal ion demand have previously been demonstrated in various models of ocular injury using MEMRI (Berkowitz et al., 2007).

Given that the rat ON myelination begins approximately 0.5 mm posterior to the sclera (Morrison, 2005), interestingly, we seemed to be able to delineate the unmyelinated ONH as a constriction between the sclera and the intraorbital ON in Fig. 6. The Mn^{2+} accumulation in the ONH may be due to uptake by glia and connective tissue cells via extra-axonal diffusion (Taylor and Weiss, 1965; Watanabe et al., 2004) since the rat lamina cribrosa is relatively sparse (Morrison, 2005). The apparent increase in accumulation of Mn^{2+} ions in the glaucomatous ONH might suggest the swelling of axons with a deposition of intracellular membranous organelles, whose fast axonal movement was expected to be disturbed at the pores of the connective tissues in the lamina cribrosa (Gross et al., 2003; Pease et al., 2000) as confirmed by light microscopic histopathology and transmission electron microscopic studies (Gross et al., 2003; Quigley, 1999). It is also possible that oxidative damage at the glaucomatous ONH would lead to more Mn^{2+} accumulations in mitochondrial superoxide dismutase (SOD-2) and catalase (Neufeld, 1999; Massaad et al., 2007).

Accumulation of Mn^{2+} in vitreous humour

Mn^{2+} might travel around in the posterior chamber by both diffusion and convection (Xu et al., 2000). Previous studies in normal primate eyes reported that intravitreal injection of similar dosages of Mn^{2+} reached the retinal boundary at 35 min after intravitreal injection, with no diffusion into the lens within the first 53 min (Li et al., 2004). The gradual reduction in signal intensities in our experiments might therefore indicate the continual clearance of Mn^{2+} away from the posterior chamber via the venous outflow, or by entering the RGCs via Ca^{2+} channels upon depolarization (Pautler, 2006) or other ion channels like divalent metal transporters (Bearer et al., 2007; Takeda, 2003).

The higher signal intensity observed in the vitreous humour in the glaucomatous eye appeared to result from the blockade of the conventional trabecular route drained by the episcleral and limbal veins upon photocoagulation. Further, the RGC loss in the current model, together with possible occlusion in the ONH (Thanos and Naskar, 2004), might reduce the uptake of Mn^{2+} ions into the intracellular space, causing an accumulation in the vitreous humour. It is apparent that the usual pattern of Mn^{2+} clearance in the glaucomatous eyeball was perturbed upon intravitreal injection.

By applying MEMRI, a global view for the investigation of chronic glaucoma within the rat primary visual system could be provided in vivo. This may complement other histological and MRI techniques to define the defective location specifically and conveniently for finer studies (Lin et al., 2001; Lin et al., 2003) and may help monitor the effect of drug interventions, e.g. the neuroprotective effect of *Lycium barbarum* Lynn (Chan et al., 2007) to the glaucoma models globally and longitudinally. In recent human studies, functional MRI has successfully demonstrated the relationship of the functional organization of primary visual cortex (V1) with the damage to the optic disc and the visual field loss in primary open-angle glaucoma (POAG) (Duncan et al., 2007a,b). Given the dependency of trans-neuronal transmission of Mn^{2+} to electrical activity (Bearer et al., 2007), further investigations should be performed to study the progression of trans-synaptic degeneration at the lateral geniculate nuclei (LGN) and the visual cortex (Lindsey et al., 2007; Gupta and Yucel, 2007) in the glaucoma models. We may also apply the commonly used BOLD and CBF functional MRI techniques to cross-correlate with the Mn^{2+}-based synaptic activity in the same animal model (Duong et al., 2000). This is of particular importance as lesions of the LGN and the visual cortex would induce loss of RGCs and the degenerating LGN in glaucoma may similarly disrupt trophic support to RGCs, adding further insult to their glaucomatous damage within the globe (Yucel et al., 2003). Experimentally, it is also desirable to increase the resolution of MRI acquisitions and the number of time points so as to better delineate the LGN as well as the SI profile along the entire rat ON, or specifically, in the superior regions of the ONs.

To conclude, MEMRI potentially provides an in vivo, longitudinal and three-dimensional means to investigate the abnormalities in the visual components of the rat model of chronic glaucoma. The delayed increase in T1-weighted signal intensity in the glaucomatous ON at 6 weeks but not 2 weeks after glaucoma induction might be suggestive of the disease progression related to RGC loss, axonal density decrease, and/or disturbance on fast axonal transport. The accumulation of Mn^{2+} ions in the vitreous humour of the glaucomatous eye could possibly arise from the perturbation of the usual pattern of Mn^{2+} clearance in the glaucomatous eyeball. High concentrations of Mn^{2+} ions were also observed at the ONH and the retina. The MEMRI approach may help understand the disease mechanisms, monitor the effect of drug interventions to glaucoma models and complement the conventional histological and electrophysiological techniques in examining the glaucomatous visual components.

Acknowledgments

The authors would like to thank Mr. Darrell Li and Mr. Matthew Cheung at Laboratory of Biomedical Imaging and Signal Processing, and Dr. Rachel Li and Ms Phillis Kau at the Department of Anatomy at The University of Hong Kong for technical assistance. This work was supported in part by Hong Kong Research Grant Council and The University of Hong Kong CRCG grant.

References

Anderson, D.R., Hendrickson, A., 1974. Effect of intraocular pressure on rapid axoplasmic transport in monkey optic nerve. Invest. Ophthalmol. 13, 771–783.

Aoki, I., Wu, Y.J., Silva, A.C., Lynch, R.M., Koretsky, A.P., 2004a. In vivo detection of neuroarchitecture in the rodent brain using manganese-enhanced MRI. Neuroimage 22, 1046–1059.

Aoki, I., Naruse, S., Tanaka, C., 2004b. Manganese-enhanced magnetic resonance imaging (MEMRI) of brain activity and applications to early detection of brain ischemia. NMR Biomed. 17, 569–580.

Banerjee, D., Hegedus, B., Gutmann, D.H., Garbow, J.R., 2007. Detection and measurement of neurofibromatosis-1 mouse optic glioma in vivo. Neuroimage 35, 1434–1437.

Bearer, E.L., Falzone, T.L., Zhang, X., Biris, O., Rasin, A., Jacobs, R.E., 2007. Role of neuronal activity and kinesin on tract tracing by manganese-enhanced MRI (MEMRI). NeuroImage.

Berkowitz, B.A., Roberts, R., Goebel, D.J., Luan, H., 2006. Noninvasive and simultaneous imaging of layer-specific retinal functional adaptation by manganese-enhanced MRI. Invest Ophthalmol Vis. Sci. 47, 2668–2674.

Berkowitz, B.A., Roberts, R., Luan, H., Bissig, D., Bui, B.V., Gradianu, M., Calkins, D.J., Vingrys, A.J., 2007. Manganese-enhanced MRI studies of alterations of intraretinal ion demand in models of ocular injury. Invest. Ophthalmol. Vis. Sci. 48, 3796–3804.

Braun, R.D., Gradianu, M., Vistisen, K.S., Roberts, R.L., Berkowitz, B.A., 2007. Manganese-enhanced MRI of human choroidal melanoma xenografts. Invest. Ophthalmol. Vis. Sci. 48, 963–967.

Chan, H.C., Chang, R.C., Koon-Ching Ip, A., Chiu, K., Yuen, W.H., Zee, S.Y., So, K.F., 2007. Neuroprotective effects of *Lycium barbarum* Lynn on protecting retinal ganglion cells in an ocular hypertension model of glaucoma. Exp. Neurol. 203, 269–273.

Chauhan, B.C., Levatte, T.L., Garnier, K.L., Tremblay, F., Pang, I.H., Clark, A.F., Archibald, M.L., 2006. Semiquantitative optic nerve grading scheme for determining axonal loss in experimental optic neuropathy. Invest Ophthalmol. Vis. Sci. 47, 634–640.

Cheng, H., Nair, G., Walker, T.A., Kim, M.K., Pardue, M.T., Thule, P.M., Olson, D.E., Duong, T.Q., 2006. Structural and functional MRI reveals multiple retinal layers. Proc. Natl. Acad. Sci. U. S. A. 103, 17525–17530.

Dandona, L., Hendrickson, A., Quigley, H.A., 1991. Selective effects of experimental glaucoma on axonal transport by retinal ganglion cells to the dorsal lateral geniculate nucleus. Invest Ophthalmol. Vis. Sci. 32, 1593–1599.

Duncan, R.O., Sample, P.A., Weinreb, R.N., Bowd, C., Zangwill, L.M., 2007a. Retinotopic organization of primary visual cortex in glaucoma: a method for comparing cortical function with damage to the optic disk. Invest Ophthalmol Vis Sci 48, 733–744.

Duncan, R.O., Sample, P.A., Weinreb, R.N., Bowd, C., Zangwill, L.M., 2007b. Retinotopic organization of primary visual cortex in glaucoma: comparing fMRI measurements of cortical function with visual field loss. Prog. Retin Eye Res. 26, 38–56.

Duong, T.Q., Silva, A.C., Lee, S.P., Kim, S.G., 2000. Functional MRI of calcium-dependent synaptic activity: cross correlation with CBF and BOLD measurements. Magn. Reson Med. 43, 383–392.

Elluru, R.G., Bloom, G.S., Brady, S.T., 1995. Fast axonal transport of kinesin in the rat visual system: functionality of kinesin heavy chain isoforms. Mol. Biol. Cell 6, 21–40.

Fu, Q.L., Wu, W., Wang, H., Li, X., Lee, V.W., So, K.F., 2007. Up-regulated endogenous erythropoietin/erythropoietin receptor system and exogenous erythropoietin rescue retinal ganglion cells after chronic ocular hypertension. Cell Mol. Neurobiol.

Gross, R.L., Ji, J., Chang, P., Pennesi, M.E., Yang, Z., Zhang, J., Wu, S.M., 2003. A mouse model of elevated intraocular pressure: retina and optic nerve findings. Trans. Am. Ophthalmol. Soc. 101, 163–169 discussion 169–171.

Grozdanic, S.D., Betts, D.M., Sakaguchi, D.S., Allbaugh, R.A., Kwon, Y.H., Kardon, R.H., 2003. Laser-induced mouse model of chronic ocular hypertension. Invest Ophthalmol. Vis. Sci. 44, 4337–4346.

Gupta, N., Yucel, Y.H., 2007. Glaucoma as a neurodegenerative disease. Curr. Opin. Ophthalmol. 18, 110–114.

Haapanen, A., Ramadan, U.A., Autti, T., Joensuu, R., Tyynela, J., 2007. In vivo MRI reveals the dynamics of pathological changes in the brains of cathepsin D-deficient mice and correlates changes in manganese-enhanced MRI with microglial activation. Magn. Reson. Imaging.

Hetling, J.R., Baig-Silva, M.S., Comer, C.M., Pardue, M.T., Samaan, D.Y., Qtaishat, N.M., Pepperberg, D.R., Park, T.J., 2005. Features of visual function in the naked mole-rat *Heterocephalus glaber*. J. Comp. Physiol. A. Neuroethol. Sens. Neural. Behav. Physiol. 191, 317–330.

Hernandez, C., Blackburn, E., Alvarez, J., 1989. Calibre and microtubule content of the non-medullated and myelinated domains of optic nerve axons of rats. Eur. J. Neurosci 1, 654–658.

Hiruma, H., Katakura, T., Takahashi, S., Ichikawa, T., Kawakami, T., 2003. Glutamate and amyloid beta-protein rapidly inhibit fast axonal transport in cultured rat hippocampal neurons by different mechanisms. J. Neurosci. 23, 8967–8977.

Johnson, E.C., Deppmeier, L.M., Wentzien, S.K., Hsu, I., Morrison, J.C., 2000. Chronology of optic nerve head and retinal responses to elevated intraocular pressure. Invest. Ophthalmol. Vis. Sci. 41, 431–442.

Kaufman, P.L., 1999. Nitric-oxide synthase and neurodegeneration/neuroprotection. Proc. Natl. Acad. Sci. U. S. A. 96, 9455–9456.

Kawai, Y., Aoki, I., Matsumoto, N., Umeda, M., Higuchi, T., Kershaw, J., Silva, A.C., Tanaka, C., 2007. Detection of reactive giosis using manganese-enhanced MRI (MEMRI). Proc. Intl. Soc. Mag. Reson. Med. 15, 2463.

Khosla, P.K., Patra, S., Prakash, P., Ratnakar, K.S., 1982. Axoplasmic transport in optic nerve (an experimental study in rabbits). Indian J. Ophthalmol. 30, 23–28.

Lau, J., Dang, M., Hockmann, K., Ball, A.K., 2006. Effects of acute delivery of endothelin-1 on retinal ganglion cell loss in the rat. Exp. Eye Res. 82, 132–145.

Leergaard, T.B., Bjaalie, J.G., Devor, A., Wald, L.L., Dale, A.M., 2003. In vivo tracing of major rat brain pathways using manganese-enhanced magnetic resonance imaging and three-dimensional digital atlasing. NeuroImage 20, 1591–1600.

Li, S.K., Jeong, E.K., Hastings, M.S., 2004. Magnetic resonance imaging study of current and ion delivery into the eye during transscleral and transcorneal iontophoresis. Invest. Ophthalmol. Vis. Sci. 45, 1224–1231.

Li, R.S., Tay, D.K., Chan, H.H., So, K.F., 2006a. Changes of retinal functions following the induction of ocular hypertension in rats using argon laser photocoagulation. Clin. Experiment Ophthalmol. 34, 575–583.

Li, R.S., Chen, B.Y., Tay, D.K., Chan, H.H., Pu, M.L., So, K.F., 2006b. Melanopsin-expressing retinal ganglion cells are more injury-resistant in a chronic ocular hypertension model. Invest Ophthalmol. Vis. Sci. 47, 2951–2958.

Lin, C.P., Tseng, W.Y., Cheng, H.C., Chen, J.H., 2001. Validation of diffusion tensor magnetic resonance axonal fiber imaging with registered manganese-enhanced optic tracts. Neuroimage 14, 1035–1047.

Lin, C.P., Wedeen, V.J., Chen, J.H., Yao, C., Tseng, W.Y., 2003. Validation of diffusion spectrum magnetic resonance imaging with manganese-enhanced rat optic tracts and ex vivo phantoms. NeuroImage 19, 482–495.

Lindsey, J.D., Scadeng, M., Dubowitz, D.J., Crowston, J.G., Weinreb, R.N., 2007. Magnetic resonance imaging of the visual system in vivo: transsynaptic illumination of V1 and V2 visual cortex. NeuroImage 34, 1619–1626.

Mabuchi, F., Aihara, M., Mackey, M.R., Lindsey, J.D., Weinreb, R.N., 2003. Optic nerve damage in experimental mouse ocular hypertension. Invest Ophthalmol Vis Sci 44, 4321–4330.

Mabuchi, F., Aihara, M., Mackey, M.R., Lindsey, J.D., Weinreb, R.N., 2004. Regional optic nerve damage in experimental mouse glaucoma. Invest. Ophthalmol. Vis. Sci. 45, 4352–4358.

Massaad, 2007. The role of mitochondrial superoxide in Alzheimer's pathology. Proc. Intl. Soc. Mag. Reson. Med. 15, 3088.

Molokhia, S.A., Jeong, E.K., Higuchi, W.I., Li, S.K., 2007. Examination of penetration routes and distribution of ionic permeants during and after transscleral iontophoresis with magnetic resonance imaging. Int. J. Pharm. 335, 46–53.

Morrison, J.C., Fraunfelder, F.W., Milne, S.T., Moore, C.G., 1995. Limbal microvasculature of the rat eye. Invest. Ophthalmol. Vis. Sci. 36, 751–756.

Morrison, J.C., Moore, C.G., Deppmeier, L.M., Gold, B.G., Meshul, C.K., Johnson, E.C., 1997. A rat model of chronic pressure-induced optic nerve damage. Exp. Eye Res. 64, 85–96.

Morrison, J.C., 2005. Elevated intraocular pressure and optic nerve injury models in the rat. J. Glaucoma 14, 315–317.

Morrison, J.C., Johnson, E.C., Cepurna, W., Jia, L., 2005. Understanding mechanisms of pressure-induced optic nerve damage. Prog Retin Eye Res 24, 217–240.

Naskar, R., Wissing, M., Thanos, S., 2002. Detection of early neuron degeneration and accompanying microglial responses in the retina of a rat model of glaucoma. Invest Ophthalmol. Vis. Sci. 43, 2962–2968.

Neufeld, A.H., 1999. Nitric oxide: a potential mediator of retinal ganglion cell damage in glaucoma. Surv. Ophthalmol. 43 (Suppl 1), S129–S135.

Pautler, R.G., 2004. In vivo, trans-synaptic tract-tracing utilizing manganese-enhanced magnetic resonance imaging (MEMRI). NMR Biomed. 17, 595–601.

Pautler, R.G., 2006. Biological applications of manganese-enhanced magnetic resonance imaging. Methods. Mol. Med. 124, 365–386.

Pautler, R.G., Silva, A.C., Koretsky, A.P., 1998. In vivo neuronal tract tracing using manganese-enhanced magnetic resonance imaging. Magn. Reson. Med. 40, 740–748.

Pease, M.E., McKinnon, S.J., Quigley, H.A., Kerrigan-Baumrind, L.A., Zack, D.J., 2000. Obstructed axonal transport of BDNF and its receptor TrkB in experimental glaucoma. Invest. Ophthalmol. Vis. Sci. 41, 764–774.

Quigley, H.A., 1999. Neuronal death in glaucoma. Prog. Retin Eye Res. 18, 39–57.

Quigley, H.A., Addicks, E.M., 1980. Chronic experimental glaucoma in primates. II. Effect of extended intraocular pressure elevation on optic nerve head and axonal transport. Invest Ophthalmol. Vis. Sci. 19, 137–152.

Quigley, H.A., Broman, A.T., 2006. The number of people with glaucoma worldwide in 2010 and 2020. Br. J. Ophthalmol. 90, 262–267.

Quigley, H.A., Guy, J., Anderson, D.R., 1979. Blockade of rapid axonal transport. Effect of intraocular pressure elevation in primate optic nerve. Arch. Ophthalmol. 97, 525–531.

Quigley, H.A., Sanchez, R.M., Dunkelberger, G.R., L'Hernault, N.L., Baginski, T.A., 1987. Chronic glaucoma selectively damages large optic nerve fibers. Invest. Ophthalmol. Vis. Sci. 28, 913–920.

Ryu, S., Brown, S.L., Kolozsvary, A., Ewing, J.R., Kim, J.H., 2002. Noninvasive detection of radiation-induced optic neuropathy by manganese-enhanced MRI. Radiat Res. 157, 500–505.

Sasaoka, M., Taniguchi, T., Shimazawa, M., Ishida, N., Shimazaki, A., Hara, H., 2006. Intravitreal injection of endothelin-1 caused optic nerve damage following to ocular hypoperfusion in rabbits. Exp. Eye Res. 83, 629–637.

Serrano, F., Terashima, T., Chan, L.C., Pautler, R.G., 2007. In vivo assessment of axonal transport in diabetic mice using manganese-enhanced MRI (MEMRI). Proc. Intl. Soc. Mag. Reson. Med. 15, 2463.

Silva, A.C., Lee, J.H., Aoki, I., Koretsky, A.P., 2004. Manganese-enhanced magnetic resonance imaging (MEMRI): methodological and practical considerations. NMR Biomed 17, 532–543.

Smith, K.D., Kallhoff, V., Zheng, H., Pautler, R.G., 2007. In vivo axonal transport rates decrease in a mouse model of Alzheimer's disease. NeuroImage 35, 1401–1408.

Song, S.K., Sun, S.W., Ju, W.K., Lin, S.J., Cross, A.H., Neufeld, A.H., 2003. Diffusion tensor imaging detects and differentiates axon and myelin degeneration in mouse optic nerve after retinal ischemia. NeuroImage 20, 1714–1722.

Sun, S.W., Liang, H.F., Le, T.Q., Armstrong, R.C., Cross, A.H., Song, S.K., 2006. Differential sensitivity of in vivo and ex vivo diffusion tensor imaging to evolving optic nerve injury in mice with retinal ischemia. NeuroImage 32, 1195–1204.

Taylor, A.C., Weiss, P., 1965. Demonstration of axonal flow by the movement of tritium-labeled protein in mature optic nerve fibers. Proc. Natl. Acad. Sci. U. S. A. 54, 1521–1527.

Takeda, A., 2003. Manganese action in brain function. Brain Res. Brain Res. Rev. 41, 79–87.

Thanos, S., Naskar, R., 2004. Correlation between retinal ganglion cell death and chronically developing inherited glaucoma in a new rat mutant. Exp Eye Res. 79, 119–129.

Thuen, M., Singstad, T.E., Pedersen, T.B., Haraldseth, O., Berry, M., Sandvig, A., Brekken, C., 2005. Manganese-enhanced MRI of the optic visual pathway and optic nerve injury in adult rats. J. Magn. Reson Imaging 22, 492–500.

Van der Linden, A., Van Meir, V., Tindemans, I., Verhoye, M., Balthazart, J., 2004. Applications of manganese-enhanced magnetic resonance imaging (MEMRI) to image brain plasticity in song birds. NMR Biomed 17, 602–612.

Van der Linden, A., Van Camp, N., Ramos-Cabrer, P., Hoehn, M., 2007. Current status of functional MRI on small animals: application to physiology, pathophysiology, and cognition. NMR Biomed. 20, 522–545.

van der Zijden, J.P., Wu, O., van der Toorn, A., Roeling, T.P., Bleys, R.L., Dijkhuizen, R.M., 2007. Changes in neuronal connectivity after stroke in rats as studied by serial manganese-enhanced MRI. NeuroImage 34, 1650–1657.

Vickers, J.C., Craig, J.E., Stankovich, J., McCormack, G.H., West, A.K., Dickinson, J.L., McCartney, P.J., Coote, M.A., Healey, D.L., Mackey, D.A., 2002. The apolipoprotein epsilon4 gene is associated with elevated risk of normal tension glaucoma. Mol. Vis. 8, 389–393.

Wang, J., Ge, J., Sadun, A.A., Lam, T.T., 2004. Characteristics of optic nerve damage induced by chronic intraocular hypertension in rat. Yan Ke Xue Bao 20, 25–29.

Watanabe, T., Michaelis, T., Frahm, J., 2001. Mapping of retinal projections in the living rat using high-resolution 3D gradient-echo MRI with Mn2+-induced contrast. Magn. Reson. Med. 46, 424–429.

Watanabe, T., Frahm, J., Michaelis, T., 2004. Functional mapping of neural pathways in rodent brain in vivo using manganese-enhanced three-dimensional magnetic resonance imaging. NMR Biomed. 17, 554–568.

WoldeMussie, E., Ruiz, G., Wijono, M., Wheeler, L.A., 2001. Neuroprotection of retinal ganglion cells by brimonidine in rats with laser-induced chronic ocular hypertension. Invest. Ophthalmol. Vis. Sci. 42, 2849–2855.

Xu, J., Heys, J.J., Barocas, V.H., Randolph, T.W., 2000. Permeability and diffusion in vitreous humour: implications for drug delivery. Pharm Res. 17, 664–669.

Yang, J., Wu, E.X., 2008. Detection of cortical gray matter lesion in the late phase of mild hypoxic-ischemic injury by manganese-enhanced MRI. NeuroImage 39, 669–679.

Yucel, Y.H., Zhang, Q., Weinreb, R.N., Kaufman, P.L., Gupta, N., 2003. Effects of retinal ganglion cell loss on magno-, parvo-, koniocellular pathways in the lateral geniculate nucleus and visual cortex in glaucoma. Prog. Retin. Eye Res. 22, 465–481.

University of Pittsburgh

Overview of our MRI Research Programme

Development and application of novel in vivo MRI contrasts to normal, developing and injured visual system. *(Imaging research)*

Monitoring damages and disease progression in visual brain
(Pathophysiology; neurobiology)

1. Early Diagnosis and prediction of disease progression in visual brain;
2. Improve understanding of eye and/or visual brain disease mechanisms;
3. Improve strategies for prevention and timely intervention of the disease for preservation of vision.

Monitoring neuroplasticity and regeneration in visual brain
(Regenerative ophthalmology; neuroscience; psychology; biomaterials; tissue engineering)

1. Improve understanding of brain mechanisms of microstructural reorganization, functional recovery and cross-modal interactions;
2. Devise strategies for visual restoration for the blind.

Improve quality of life for the visually impaired.